2009

Zero-propellant maneuver guidance

Bedrossian, Nazareth S.; Bhatt, Sagar; Kang, Wei; Ross, Michael I.

IEEE

Bedrossian, N., Bhatt, S., Kang, W. & Ross, I.M. 2009, "Zero-propellant maneuver guidance", IEEE Control Systems Magazine, vol. 29, no. 5, pp. 53-73.
https://hdl.handle.net/10945/56999

COURTESY OF NASA

Zero-Propellant Maneuver Guidance

ROTATING THE INTERNATIONAL SPACE STATION WITH COMPUTATIONAL DYNAMIC OPTIMIZATION

BY NAZARETH S. BEDROSSIAN, SAGAR BHATT, WEI KANG, and I. MICHAEL ROSS

To maintain its orbit and control its attitude, the International Space Station (ISS) is equipped with thrusters as well as four control moment gyroscopes (CMGs). The CMGs can be used only for attitude control, while the thrusters can be used for either attitude control or orbit corrections. For attitude control, thrusters can complete reorientations much more rapidly than the CMGs since the torque capability of the thrusters is at least an order of magnitude larger than the torque capability of the CMGs. However, using thrusters has significant disadvantages, such as consumption of propellant, solar array contamination, and stressing of the ISS structure. CMGs can avoid these disadvantages as long as they operate within their angular momentum capacity because they are powered by electricity generated by the ISS solar arrays. If the CMG momentum becomes saturated, that is, the total angular momentum of the CMGs reaches its maximum value, the control authority of the CMGs is considered lost. For further information about CMGs and saturation, see "CMGs, Momentum Saturation, and Robotics Analogy." Even at a slow rate of rotation, large-angle ISS maneuvers performed with CMGs can result in momentum saturation because the CMGs must compensate for the environmental disturbance torques on the ISS along the flight-software-generated attitude trajectory. As a result, until 2006 all large-angle ISS rotations were performed using thrusters.

However, this situation changed with the development and flight test of a guidance approach referred to as zero-propellant maneuver (ZPM), which can perform large-angle ISS rotations without saturating the CMGs. On November 5, 2006 [1], [2], the CMGs commanded by ZPM guidance

Digital Object Identifier 10.1109/MCS.2009.934089

1066-033X/09/$26.00©2009IEEE

CMGs, Momentum Saturation, and Robotics Analogy

A control moment gyroscope (CMG) is a momentum-storage device used to control spacecraft attitude. Angular momentum of a fixed magnitude is generated by spinning a rotor at a constant rate using an electric motor. The spinning rotor is mounted in a gimbal assembly that can be rotated about multiple axes. By changing the direction of its angular momentum vector, a CMG can generate a torque on the spacecraft. The maximum torque that a CMG can generate is limited by the peak rate at which the electric motors can rotate its gimbals. Comparing CMGs with reaction wheels, CMG rotors have a fixed spin but a variable spin axis, whereas reaction wheel rotors have a fixed spin axis but a variable spin rate. CMGs are classified based on the number of gimbals used, single gimbal or double gimbal. A model for a double-gimbal CMG is shown in Figure S1. The ISS uses double-gimbal CMGs as shown in Figure S2. Each ISS CMG can store 3500 ft-lbf-s of momentum when spinning at the nominal rate of 6600 rev/min [S1].

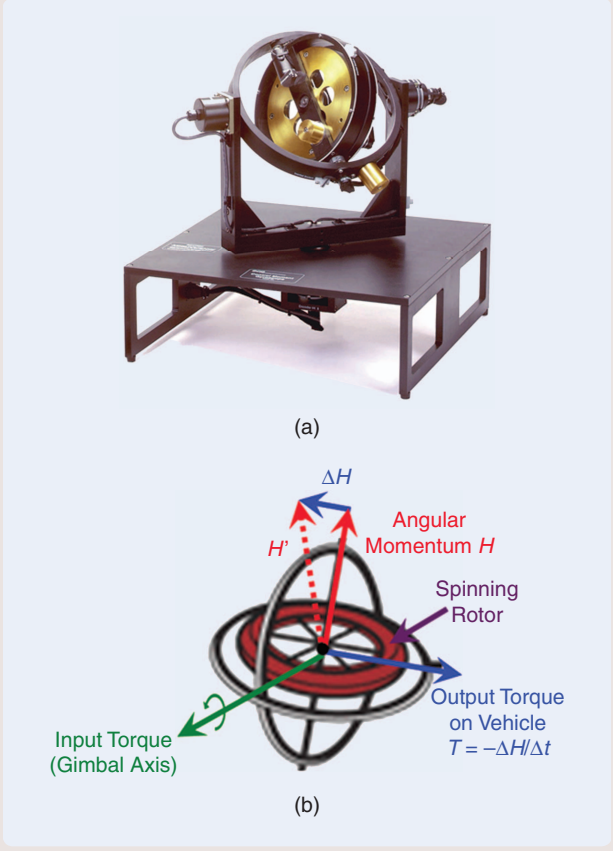

FIGURE S1 Control moment gyroscope (CMG). A CMG consists of (a) a rotor spinning at a constant rate mounted in gimbals that alter the spin axis of the rotor. Changing the direction of the CMG angular momentum vector by rotation about the gimbal axis produces (b) an output torque perpendicular to both the CMG momentum vector and the gimbal axis. [(a) is used with permission from Educational Control Products.]

The total angular momentum of a CMG cluster is the vector sum of the individual CMG momenta. For a cluster of n double-gimbal CMGs, the total angular momentum vector $\mathrm{H}_{\mathrm{CMG}} \in \mathcal{R}^3$ is [S2]

$$\mathrm{H}_{\mathrm{CMG}}(\theta) = \sum_{i=1}^{n} \mathrm{H}_i(\theta), \tag{S1}$$

where $\mathrm{H}_i(\theta)$is the momentum vector for the ith CMG, and $\theta \in \mathcal{R}^{2n}$ is the gimbal angle vector. The total torque $\mathrm{T}_{\mathrm{CMG}} \in \mathcal{R}^3$ produced by the CMG cluster is the rate of change of $\mathrm{H}_{\mathrm{CMG}}(\theta)$. This vector is obtained by differentiating (S1), which yields

$$\mathrm{T}_{\mathrm{CMG}}(\theta, \dot{\theta}) = \sum_{i=1}^{2n} \frac{\partial \mathrm{H}_i(\theta)}{\partial \theta} \dot{\theta} = \mathrm{J}_{\mathrm{CMG}}(\theta)\dot{\theta}, \tag{S2}$$

where $J_{\mathrm{CMG}}\mathcal{R}^{3\times 2n}$ is the CMG kinematics Jacobian matrix. The maximum torque the cluster can generate is obtained by taking the norm of (S2)

$$\|\mathrm{T}_{\mathrm{CMG}}(\theta, \dot{\theta})\|_\infty \leq \|J_{\mathrm{CMG}}(\theta)\|_{\mathrm{ind}\infty} \|\dot{\theta}\|_\infty,$$

where the vector and induced matrix norms are given by $\|\theta\|_\infty = \max_{1\leq i\leq 2n} |\theta_i|$, and $\|J\|_{\mathrm{ind}\infty} = \max_{1\leq k\leq 3} \sum_{l=1}^{2n} |J_{k,l}|$, respectively [S3]. Both the total cluster momentum and total cluster torque can saturate. During momentum saturation, the cluster momentum cannot increase in a particular direction. Analogously, during torque saturation, the cluster torque cannot increase in a particular direction.

We can provide an intuitive explanation of the relationship between double-gimbal CMG momentum and torque saturation by means of a robotics analogy for CMGs [S2]. Consider the end-effector location for an n-link revolute joint robotic manipulator,

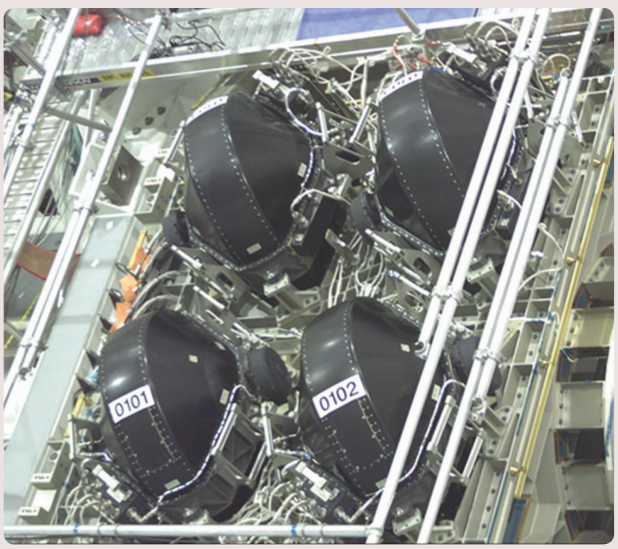

FIGURE S2 International Space Station (ISS) control moment gyroscopes (CMGs). Zero-propellant maneuvers for the ISS are accomplished by using up to four double-gimbal parallel-mounted CMGs. (Used with permission from JAXA.)

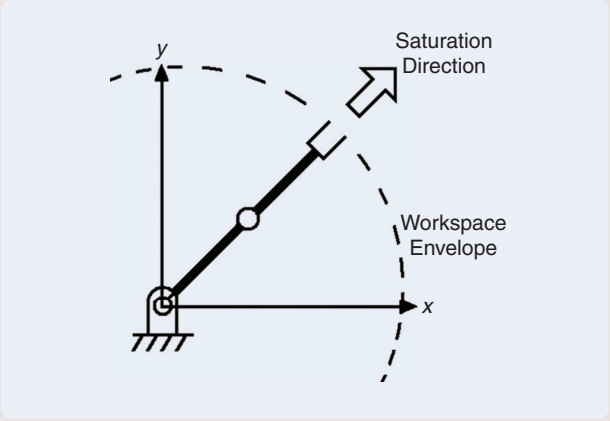

FIGURE S3 Robotic analogue for control moment gyroscope (CMG) momentum saturation. CMG saturation can be explained using a robotic manipulator that is extended maximally in a certain direction. The collection of all maximally extended end-effector locations is the manipulator workspace envelope. Just as the manipulator cannot extend past the workspace envelope, the CMG momentum also cannot increase past the momentum envelope. Momentum saturation implies torque saturation in the radial direction.

which can be expressed as the vector sum of individual link displacements [S4]

$$X_{\text{rbx}}(q) = \sum_{i=1}^{n} X_i(q_i), \tag{S3}$$

where $X_{\text{rbx}} \in \mathcal{R}^3$ is the location of the end-effector, $q \in \mathcal{R}^n$ is the joint-angle vector, and, for link i, X_i is the displacement and q_i is the joint angle. Differentiating (S3) yields

$$\dot{X}_{rbx}(q, \dot{q}) = \sum_{i=1}^{n} \frac{\partial X_i(q_i)}{\partial q_i} \dot{q}_i = J_{rbx}(q)\dot{q}, \tag{S4}$$

where $J_{\text{rbx}} \in \mathcal{R}^{3\times n}$ is the manipulator Jacobian, and $\dot{q} \in \mathcal{R}^n$ is the joint rate vector. The maximum end-effector velocity is obtained by taking the norm of (S4)

$$\|\dot{X}_{\text{rbx}}(q, \dot{q})\|_\infty \leq \|J_{\text{rbx}}(q)\|_{\text{ind}\infty} \|\dot{q}\|_\infty.$$

By comparing (S1), (S2) with (S3), (S4), manipulator links are analogous to individual CMG momentum. Hence, the manipulator end-effector position is analogous to total cluster momentum, while end-effector velocity corresponds to total cluster torque. Therefore, momentum saturation is analogous to a robotic manipulator that cannot be extended farther. A simple example is shown in Figure S3 for a planar two-link manipulator. The robotic manipulator end-effector position saturation condition in terms of the saturation direction $s_{\text{rbx}} \in \mathcal{R}^3$ is given by [S4]

$$s_{\text{rbx}}^T X_{\text{rbx}} = \max_q [s_{\text{rbx}}^T X_{\text{rbx}}(q)], \tag{S5}$$

while the end-effector velocity saturation condition can be derived by differentiating (S5) to obtain

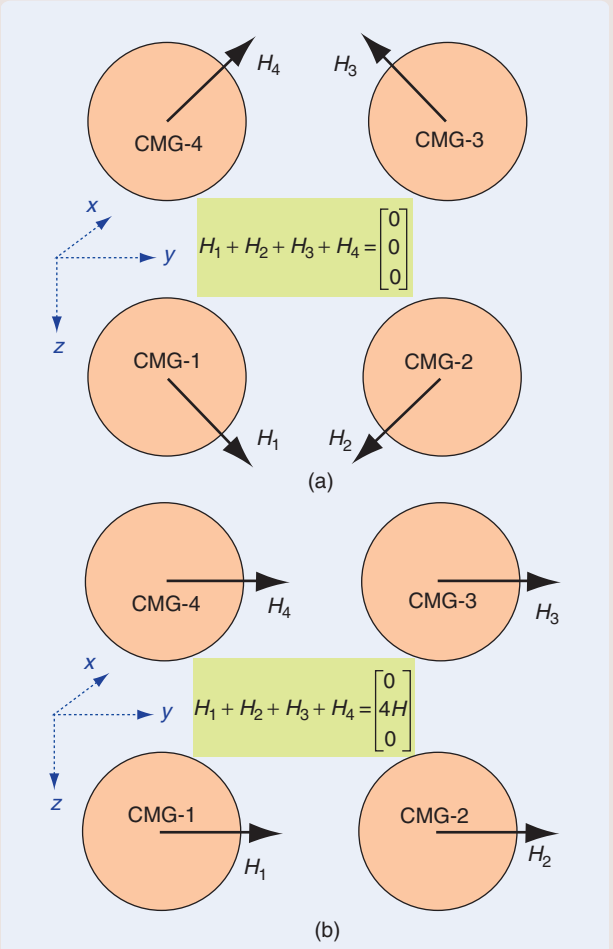

FIGURE S4 International Space Station control moment gyroscope (CMG) cluster momentum example for (a) zero total momentum and (b) maximum total momentum in the Y-direction. Each CMG stores an equal magnitude of momentum (H). In both examples the momentum vector for each CMG lies in the Y-Z plane. In (b), all of the CMG rotors are aligned, and thus the total momentum cannot increase in the Y-direction. Hence in this configuration, the CMG momentum is saturated.

$$s_{\text{rbx}}^T \dot{X}_{\text{rbx}} = 0. \tag{S6}$$

Similarly, the total cluster momentum saturation condition is given by [S2]

$$s_{\text{CMG}}^T H_{\text{CMG}} = \max_\theta [s_{\text{CMG}}^T H_{\text{CMG}}(\theta)], \tag{S7}$$

while the total cluster torque saturation condition can be derived by differentiating (S7) to obtain

$$s_{\text{CMG}}^T \dot{H}_{\text{CMG}} = 0. \tag{S8}$$

Returning to the CMG case, for double-gimbal CMGs, the total cluster momentum volume is spherical, and its surface represents the momentum envelope or boundary of maximum momentum

in each direction. The total momentum of the CMG cluster depends on the gimbal angles. For example, orienting each CMG as shown in Figure S4(a) results in zero total momentum, while the CMG cluster configuration shown in Figure S4(b) results in momentum saturation in the +Y direction.

When a CMG cluster is momentum saturated, spacecraft attitude control capability with CMGs is considered lost. To recover CMG attitude control capability, thrusters are used to maintain attitude while the individual CMGs are reoriented to decrease the total momentum magnitude. This process is called CMG desaturation. If thrusters are not used to hold attitude, commanding the CMGs away from a saturated state creates a disturbance torque that changes the spacecraft attitude. Although CMG momentum saturation is generally equated with loss of attitude control capability, the robotic analogue in Figure S3 illustrates the directional nature of saturation. While motion in the saturation direction is not possible, the manipulator can move in another direction. Similarly, even though the CMGs reach momentum saturation, attitude control capability is lost only in a particular direction.

REFERENCES

[S1] L3 communications website. DGCMG 4800/250 double gimbal control moment gyro, 2002. [Online]. Available: http://www.l-3com.com/products-services/docoutput.aspx?id=445.

[S2] N. Bedrossian, J. Paradiso, E. Bergmann, and D. Rowell, "Redundant single gimbal control moment gyroscope singularity analysis," *J. Guid. Control Dyn.,* vol. 13, no. 6, pp. 1096–1101, Nov./Dec. 1990.

[S3] M. Vidyasagar, *Nonlinear Systems Analysis, 2nd ed.* Philadelphia, PA: SIAM, 2002.

[S4] W. A. Wolovich, *Robotics: Basic Analysis and Design.* New York: Holt, Rinehart and Winston, 1987.

[S5] N. Bedrossian, "Classification of singular configurations for redundant manipulators," in *Proc. IEEE Robotics and Automation Conf.,* May 13–18, 1990, vol. 2, pp. 818–823.

were used to perform a 90° rotation of the ISS configuration shown in Figure 1(a), followed by a 180° rotation on March 3, 2007 [3], [4] for the ISS configuration shown in Figure 1(b). The identical 180° reorientation performed with thrusters on January 2, 2007 consumed 110 lbm of propellant at an estimated cost of US$1,100,000. Combined, the two ZPMs saved approximately US$1,500,000 in propellant costs. This performance was achieved by commanding a momentum-optimal attitude trajectory given by the ZPM guidance command, which was generated using computational dynamic optimization. The ZPM avoids momentum saturation because the attitude trajectory is shaped so that the environmental disturbance torques are exploited to desaturate the CMGs.

The large-angle ISS maneuvers were performed with the CMGs using the architecture shown in Figure 2. The feedback controller stabilizes the system about a specified set of operating points, while the reference signal commands the system to the final state in a specified manner. Feedback control maintains the system near the operating point in spite of off-nominal initial conditions,

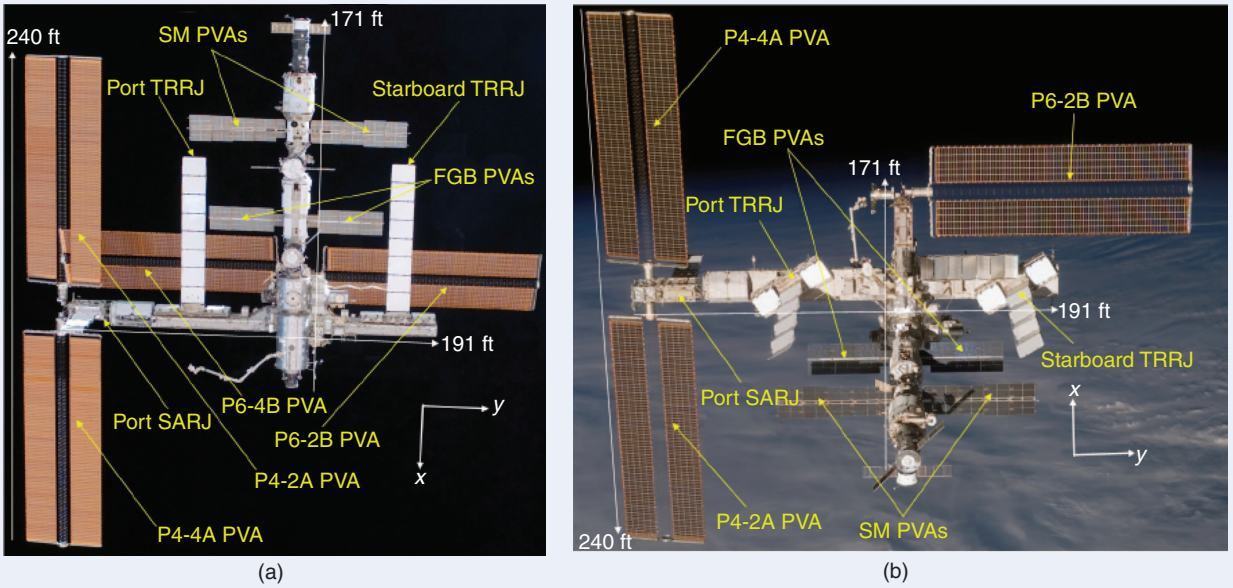

FIGURE 1 International Space Station (ISS) configurations for the two zero-propellant-maneuver (ZPM) flight demonstrations. The November 5, 2006 90° ZPM ISS configuration is shown in (a). The March 3, 2007 180° ZPM ISS configuration is shown in (b). For the 90° ZPM, the FGB PVAs (Russian Functional Cargo Block photovoltaic arrays), SM PVAs (Russian Service Module photovoltaic arrays), and P6 PVAs were rotating. For the 180° ZPM, all arrays were rotating, including the solar array rotary joint (SARJ) and thermal radiator rotary joints (TRRJs). (With permission of NASA.)

parameters, and disturbances. However, feedback is fundamentally a reactive process because errors must first appear before corrective action can take place. Hence, large-angle ISS maneuvers performed using only feedback saturate the CMGs because saturation cannot be anticipated. In contrast, the large-angle ISS maneuvers described in this article were performed without saturating the CMGs by using ZPM momentum-optimal trajectories, which provide the commands for the feedback controller to follow. This optimal trajectory is referred to as ZPM guidance. The ZPM trajectories were developed using computational dynamic optimization, which models the environmental disturbance torques to predict when CMG momentum saturation would occur along a candidate trajectory, and modifies the trajectory to maintain the CMGs within their momentum capacity. The preplanned ZPM trajectory is composed of attitude commands, which are used to achieve a rotational state transition. The rotational state includes the spacecraft attitude and rate as well as the total CMG momentum. Since onboard implementation is not feasible for legacy systems such as the ISS, a ground-developed ZPM reference trajectory is uploaded. With ZPM optimal guidance and CMG actuators, rotational state transitions that can be performed without using propellant include large-angle maneuvers [1], [3], attitude control with momentum-saturated CMGs [5], momentum desaturation [6], and rate damping [5]. Additionally, ZPM trajectories can reduce propellant consumption when only thrusters are used as actuators.

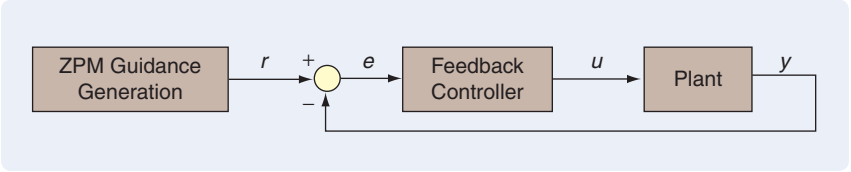

FIGURE 2 Zero-propellant maneuver (ZPM) guidance architecture. The ZPM guidance commands are designed offline to avoid control moment gyroscope momentum saturation and are uploaded to the International Space Station buffer for use as the reference signal *r*. The error *e* is computed by subtracting the output *y* from the reference signal *r*, while the feedback controller determines the control *u* required to eliminate the error.

This article describes ZPM and its applications to the ISS. First, CMG attitude maneuvers are explained, and the ISS attitude dynamics and control systems are introduced. Then the ISS nonpropulsive guidance problem and its solution are described along with implementation issues and flight results. Finally, additional examples are provided to illustrate the capabilities of ZPM.

CMG EIGENAXIS ATTITUDE MANEUVERS

To perform reorientations with CMGs, spacecraft typically use an eigenaxis maneuver logic to generate the attitude and rate commands for the feedback controller to follow. The maneuver logic is based on Euler's theorem (Figure 3), which states that an arbitrary rotation of a rigid body can be achieved by rotating through a specific angle about a fixed axis [7]. This axis is called the eigenaxis, while the eigenangle is the smallest angle rotation about the eigenaxis that reorients a body from one attitude to another. Typically, the maneuver logic generates a sequence of attitude commands by incrementally rotating about the eigenaxis at a constant rate, referred to as the maneuver rate. For this reason, we refer to these types of maneuvers as constant-rate eigenaxis maneuvers. The ISS maneuver logic uses an instantaneous rate change to start and end the rotation.

Eigenaxis trajectories are generated without taking into account environmental disturbance torques such as gravity, aerodynamic, magnetic, and solar radiation [7]. To follow the eigenaxis trajectory, the CMGs must absorb the momentum generated by the disturbance torques during the maneuver. If this disturbance momentum exceeds the capacity of the CMGs, then the CMGs can saturate regardless of the rate of rotation. Saturation can also occur when performing high-rate maneuvers even in the absence of environmental disturbance torques. Since the angular momentum of a body is proportional to its rotation rate, the CMGs must transfer more momentum to the body to rotate it faster. If the change in momentum is more than the capacity of the CMGs, then the CMGs saturate. Finally, if there are no disturbance torques but the eigenaxis is not a principal axis, then the CMGs must counteract gyroscopic effects.

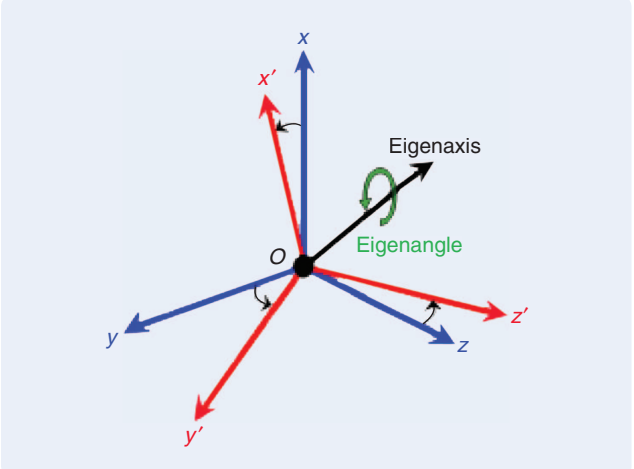

FIGURE 3 Eigenaxis and eigenangle. Euler's rotation theorem states that an arbitrary rotation of a rigid body can be performed by rotating about a body-fixed axis. The rotation axis is called the eigenaxis, while the eigenangle is the smallest angle of rotation about the eigenaxis that reorients the body from the initial attitude to the final attitude. Most spacecraft rotations are performed about the eigenaxis because it is simple to implement in flight software and is the shortest kinematic path. However, to follow the eigenaxis path, the controller must overcome environmental disturbance torques, which may saturate the control moment gyroscopes.

For spacecraft in high-Earth orbits, such as geosynchronous satellites, environmental disturbance torques are usually small [7] and can thus be neglected. Then, the inertial angular momentum of the combined system is conserved, that is,

$$\dot{\mathrm{H}}_{\mathrm{SC}} + \dot{\mathrm{H}}_{\mathrm{CMG}} = 0, \tag{1}$$

where H_{SC} is the spacecraft inertial angular momentum and $\mathrm{H}_{\mathrm{CMG}}$ is the CMG inertial angular momentum. To perform an eigenaxis reorientation, the CMGs torque the vehicle to achieve the specified maneuver rate about the eigenaxis. Since momentum is the time integral of torque and since the net change in total angular momentum is zero, it follows that

$$\Delta\mathrm{H}_{\mathrm{SC}} = -\Delta\mathrm{H}_{\mathrm{CMG}}, \tag{2}$$

where the change in spacecraft angular momentum, denoted by $\Delta\mathrm{H}_{\mathrm{SC}}$, is equal and opposite to the change in momentum $\Delta\mathrm{H}_{\mathrm{CMG}}$ of the CMGs. Since $\|\Delta\mathrm{H}_{\mathrm{SC}}\| \propto \|\Delta\omega_{\mathrm{SC}}\|$, where $\Delta\omega_{\mathrm{SC}}$ is the spacecraft inertial angular rate change, the momentum capacity of the CMGs limits the spacecraft rate change that can be achieved. Therefore, there is a maximum rate at which the spacecraft can be rotated without causing CMG momentum saturation. This situation can be avoided by rotating at a slow enough rate to operate the CMGs below their momentum capacity. When the momentum capacity is sized appropriately and rotations are planned judiciously, spacecraft can be reoriented with only momentum-storage devices and without the need for momentum desaturation using thrusters. To illustrate this point, a 90° yaw eigenaxis rotation from an initial attitude of [13 −9 2] degrees to a final attitude of [−90 −8 −2] degrees (yaw-pitch-roll order and sequence) is simulated for an ISS-sized spacecraft in geostationary orbit. Figure 4 shows that the CMG-only maneuver is completed in 21,000 s with momentum remaining below 50% of capacity. Because the disturbance torques are negligible, the final CMG momentum is close to the initial value.

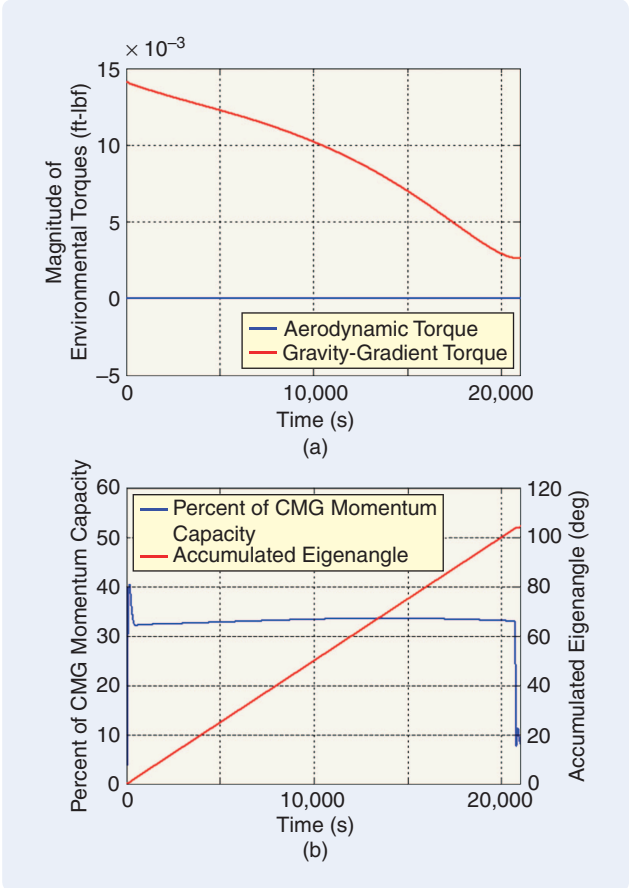

FIGURE 4 Simulated 90° yaw eigenaxis maneuver in geostationary orbit using control moment gyroscopes (CMGs). At high orbital altitudes, such as in this example, (a) environmental torques are negligible and (b) eigenaxis maneuvers can be performed at a sufficiently slow rate to avoid saturating the CMGs.

For spacecraft in low-Earth orbit, environmental disturbance torques are not negligible and cause bias momentum to accumulate even when the eigenaxis rotation is performed at a slow rate. During the rotation, the disturbance torque must be absorbed by the CMGs to maintain the spacecraft on the eigenaxis path. Because of disturbance torques, momentum is not conserved, and thus (1) becomes

$$\dot{\mathrm{H}}_{\mathrm{SC}} + \dot{\mathrm{H}}_{\mathrm{CMG}} = T_{\mathrm{dist}}, \tag{3}$$

where T_{dist} is the disturbance torque expressed in an inertial reference frame. To illustrate how disturbance torques can saturate the CMGs, a 90° eigenaxis maneuver from an initial attitude of [13−9 2] degrees to a final attitude of [−90 −8 −2] degrees (yaw-pitch-roll order and sequence) using only CMGs is simulated (Figure 5) for an ISS-sized spacecraft in low-Earth orbit. The momentum state starts at zero, similar to the example in Figure 4, but the environmental aerodynamic and gravity gradient torques along the eigenaxis path cause the CMGs to accumulate momentum. As a result, CMG saturation is reached 6500 s into the maneuver when the spacecraft has rotated 30°. At that point, CMG attitude control is lost, and the accumulated eigenangle increases past the target as the spacecraft begins to tumble.

ISS DYNAMICS WITH CMGs

Since the ISS is in low-Earth orbit at an altitude of 300 km, it experiences environmental disturbances that depend on attitude. To see the attitude dependence of these disturbances, we express (3) in an ISS body-fixed frame whose origin is the ISS center of mass [7]

$$\dot{\mathrm{H}}_{\mathrm{ISS}} + \omega_{\mathrm{ISS}} \times \mathrm{H}_{\mathrm{ISS}} + \dot{\mathrm{H}}_{\mathrm{CMG}} + \omega_{\mathrm{ISS}} \times \mathrm{H}_{\mathrm{CMG}} = \mathrm{T}_{\mathrm{dist}}, \tag{4}$$

The ZPM avoids momentum saturation because the attitude trajectory is shaped so that the environmental disturbance torques are exploited to desaturate the CMGs.

where ω_{ISS} is the inertial angular velocity of the ISS body frame, $H_{ISS} = J\omega_{ISS}$, J is the ISS time-varying inertia matrix, and all quantities are expressed in the ISS body frame. The primary disturbances $T_{dist} = T_{grav} + T_{aero}$ are due to gravity and aerodynamics. The gravity torque is due to the gravity gradient, that is, differences in gravitational force experienced by the ISS. Since the gravitational force is inversely proportional to the distance from the Earth, the parts of the ISS that are nearest the Earth experience a stronger gravitational pull. Under appropriate assumptions, the gravity torque is expressed as [7]

$$T_{grav} = 3\omega_{orb}^2 c_3 \times Jc_3,$$

where ω_{orb} is the orbital rotation rate, and c_3 is the orbit radius unit vector expressed in the ISS body frame and depends on the ISS attitude. The aerodynamic drag force also creates a torque on the ISS that depends on the angle between the spacecraft surfaces and the air stream. A simplified model for aerodynamic torque T_{aero} is given by [8]

$$T_{aero} = -r_{cp} \times \frac{1}{2}\rho C_d V^2 |A_p| c_1,$$

where r_{cp} is the center of pressure with respect to the center of mass, A_p is the projected area perpendicular to the air stream, ρ is the atmospheric density, C_d is the drag coefficient, V is the magnitude of the spacecraft translational velocity relative to the atmosphere, and c_1 is the unit ISS velocity vector expressed in the ISS body frame and thus depends on the ISS orientation.

CMG Attitude Control

From (4), we see that CMGs can apply a torque on the ISS in two ways. The first, $\omega_{ISS} \times H_{CMG}$, is the gyroscopic torque generated by the total CMG momentum. The second, $\dot{H}_{CMG}$, is the torque generated directly by the CMGs. It is interesting to note that, due to the term $\omega_{ISS} \times H_{CMG}$, CMGs can generate a bias gyroscopic torque even when $\dot{H}_{CMG} = 0$. Being directly controllable, CMG torque provides the means by which an attitude control law can be implemented.

The ISS CMG feedback control law is given by

$$\dot{H}_{CMG} = u - \omega_{ISS} \times H_{CMG}, \quad (5)$$

$$u = J[K_P \varepsilon_{err} + K_D \omega_{err}], \quad (6)$$

where K_P and K_D are the scalar proportional (P) and derivative (D) gains of the PD controller, and ε_{err} and ω_{err} are the attitude and rate command-following errors. Once the desired terminal attitude is uploaded to the ISS, the onboard flight software uses a constant-rate eigenaxis logic to generate a sequence of attitude and rate commands based on the user-specified scalar maneuver rate.

Since the commands to the CMG controller determine the accumulated CMG momentum, our goal is to develop attitude command trajectories that can expand the CMG operational envelope without saturating the CMGs.

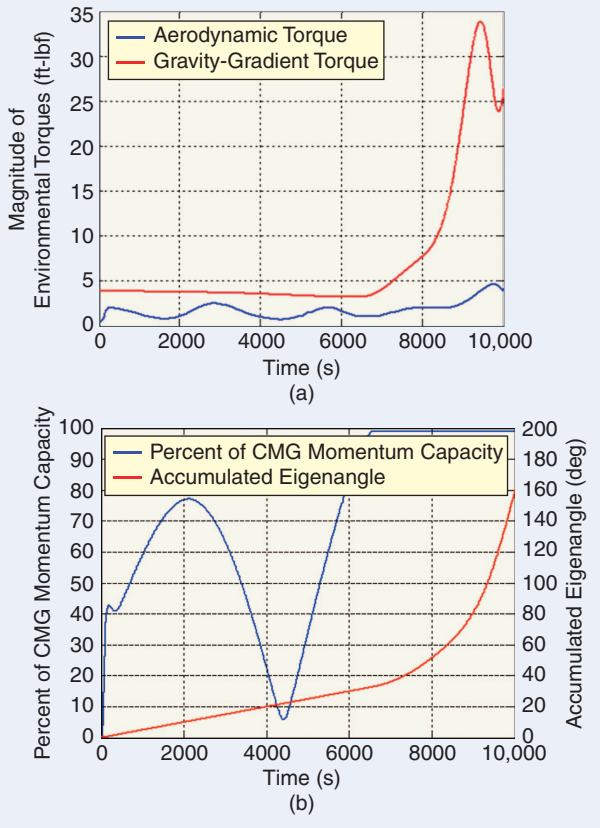

FIGURE 5 Simulated 90° yaw eigenaxis maneuver in low-Earth orbit using control moment gyroscopes (CMGs). When following an eigenaxis path, (a) environmental disturbances, including gravity gradient and aerodynamic torques, cause CMG momentum to accumulate until (b) the CMGs saturate.

Pseudospectral Dynamic Optimization

Dynamic optimization problems can be solved numerically using pseudospectral (PS) methods, which discretize the problem at selected nodes based on orthogonal functions. For example, the Legendre PS method [S6]–[S9] uses Legendre-Gauss-Lobatto (LGL) points and Legendre polynomials. Let

$$L_N(\tau) = \frac{1}{2^N N!}\frac{d^N}{dt^N}(\tau^2 - 1)^N$$

be the Legendre polynomial of degree N on the interval $[\tau_0, \tau_N] = [-1, 1]$. Then the LGL points are given by τ_0, τ_N, and the zeros $\tau_1, \ldots, \tau_{N-1}$ of the derivative $\dot{L}_N$. The spacing of these nodes for $N = 9$ is shown in Figure S5. Note that the nodes are closer together at the beginning and end compared to the middle. This feature is beneficial in many engineering applications since it captures more information during the critical times. For an arbitrary time interval $[t_0, t_f]$, the transformation $t:[\tau_0, \tau_N] = [-1, 1] \rightarrow [t_0, t_f]$ given by [S6]

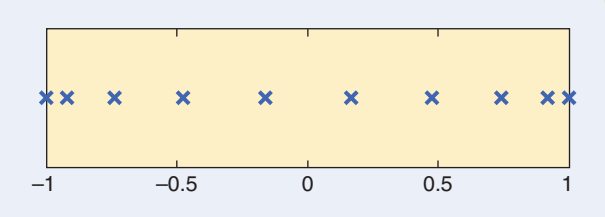

FIGURE S5 Legendre-Gauss-Lobatto (LGL) point spacing for ten nodes. In the Legendre pseudospectral optimal control method, the quantities of interest are approximated at the LGL nodes. The closer spacing of these nodes near the interval endpoints is advantageous for capturing more information during the critical times.

$$t(\tau) = \frac{(t_f - t_0)\tau + (t_f + t_0)}{2}$$

can be used to shift the LGL points to the desired interval.

Using the LGL points, the state function $x(t)$ and control function $u(t)$ are approximated by the expansions

$$x(t) \approx x^N(t(\tau)) = \sum_{i=0}^{N} x_i \phi_i(\tau),$$
$$u(t) \approx u^N(t(\tau)) = \sum_{i=0}^{N} u_i \psi_i(\tau),$$

where x_i and u_i are coefficients, ϕ_i are order N Lagrange polynomials satisfying the Kronecker-delta condition

$$\phi_i(\tau_k) = \begin{cases} 1, & \text{if } i = k, \\ 0, & \text{if } i \neq k, \end{cases}$$

and ψ_i are functions that also satisfy this condition. The coefficients x_i and u_i are then given by the values of the states and controls at the node points, that is,

$$x_i = x^N(t(\tau_i)) = x(t(\tau_i)),$$
$$u_i = u^N(t(\tau_i)) = u(t(\tau_i)).$$

PS methods are efficient for several reasons related to accuracy and simplicity. For differentiation, the derivatives of the state functions at the LGL nodes can be computed by

$$\dot{x}(t(\tau_k)) \approx \dot{x}^N(t(\tau_k)) = \frac{dx^N}{d\tau}\frac{d\tau}{dt}\bigg|_{\tau_k} = \frac{2}{(t_f - t_0)}\sum_{i=0}^{N} x_i \dot{\phi}_i(\tau_k),$$

ZERO-PROPELLANT-MANEUVER OPTIMAL GUIDANCE

The above discussion shows that the performance of the PD controller (4)–(5) depends on the command signal. We thus use computational dynamic optimization to develop a reference signal that avoids momentum saturation. The key is to time-coordinate and attitude-modulate environmental torques by shaping the attitude trajectory. Time coordination is accomplished by varying the maneuver rate, that is, speeding up or slowing down. Attitude modulation is achieved by commanding attitude excursions from an eigenaxis path. The application of this concept is referred to as a ZPM. A ZPM is a special attitude trajectory that takes advantage of environmental disturbance torques to maintain CMGs within their operational limits, thereby avoiding momentum desaturation using thrusters.

Related work can be traced back to the Skylab program, where gravity gradient torque produced by two-axis attitude maneuvers was used to desaturate momentum accumulated during the daylight portion of the orbit [9], [10]. Other applications of using gravity gradient torque to desaturate CMG momentum are considered in [11]–[13]. The common thread in these approaches is the use of small-angle approximations in the gravity gradient torque model to compute the momentum-desaturation maneuver. The approach considered in [14] minimizes fuel use by optimizing the attitude command trajectory based on nonlinear system dynamics. Although a 90° ISS yaw maneuver is performed in [14] without using propellant, the CMGs are saturated at the end of the maneuver. Optimal spacecraft maneuvers using thrusters and to a lesser extent CMGs are considered in [15] and [16]; however, environmental disturbance torques are not considered. An early application of ZPM was to solve for a CMG maneuver between specified attitudes while avoiding momentum saturation during ISS robotic payload operations and reducing the final CMG momentum magnitude by using environmental disturbance torques [17]. A more recent application used ZPM to desaturate arbitrary three-axis momentum without using thrusters by exploiting environmental disturbance torques [6]. Finally, the general rotational state transition

$$= \frac{2}{(t_f - t_0)} \sum_{i=0}^{N} D_{ki} x_i$$

using the $(N+1)\times(N+1)$ differentiation matrix D associated with the Legendre polynomials

$$D_{ki} = \begin{cases} \dfrac{L_N(t_k)}{L_N(t_i)(t_k - t_i)}, & \text{if } k \neq i, \\ -\dfrac{N(N+1)}{4}, & \text{if } k = i = 0, \\ \dfrac{N(N+1)}{4}, & \text{if } k = i = N, \\ 0, & \text{otherwise.} \end{cases}$$

Thus, the differential equation of the control system is approximated by algebraic equations at the LGL nodes. Then, numerical integration of the cost function $\int_{t_0}^{t_f} F(x(t), u(t))dt$ is performed using the Gauss-Lobatto rule

$$\int_{t_0}^{t_f} F(x(t), u(t))dt \approx \frac{(t_f - t_0)}{2} \sum_{i=0}^{N} F(x_i, u_i) w_i$$

where the LGL weights are given by

$$w_i = \frac{2}{N(N+1)[L_N(\tau_i)]^2}.$$

Since path constraints are enforced only at the nodes, the problem is transformed into finding values of the states and controls at the nodes that satisfy algebraic constraints. PS methods can approximate continuous functions with few nodes. For smooth solutions, the accuracy of these methods means that the interpolation error decreases faster than polynomial rates as the number of nodes increases.

PS methods have several mathematical properties that are useful in practice. The covector mapping theorem [S6], [S8] facilitates optimality verification and validation of the computed solution by direct application of the necessary conditions. Several theorems guarantee the feasibility and convergence of the Legendre PS method [S8], [S9]. These results are useful for problems in which safety and robustness are crucial. A Matlab [S10] implementation of the Legendre PS dynamic optimization method is available as the commercial software package DIDO [18], while a Fortran implementation by NASA is available under OTIS [S11].

REFERENCES

[S6] F. Fahroo and I. M. Ross, "Costate estimation by a Legendre pseudospectral method," *J. Guid. Control Dyn.,* vol. 24, no. 2, pp. 270–277, 2001.

[S7] J. P. Boyd, *Chebyshev and Fourier Spectral Methods.* New York: Dover, 2000.

[S8] Q. Gong, I. M. Ross, W. Kang, and F. Fahroo, "Connections between the covector mapping theorem and convergence of pseudospectral methods for optimal control," *J. Comput. Optim. Applicat.*, vol. 41, no. 3, pp. 307–335, 2008.

[S9] W. Kang, Q. Gong, and I. M. Ross, "On the convergence of nonlinear control using pseudospectral methods for feedback linearizable systems," *Int. J. Robust Nonlinear Control,* vol. 17, pp. 1251–1277, 2007.

[S10] The MathWorks, Inc. Matlab software package, 2005. [Online]. Available: http://www.mathworks.com.

[S11] S. W. Paris, J. P. Riehl, and W. K. Sjaw, "Enhanced procedures for direct trajectory optimization using nonlinear programming and implicit integration," in *Proc. AIAA/AAS Astrodynamics Specialist Conf. and Exhibit,* Keystone, CO, Aug. 21–24, 2006, AIAA 2006-6309, pp. 1–19.

was addressed and demonstrated by means of a flight test on the ISS in [1].

OPTIMAL TRAJECTORY PROBLEM FORMULATION

To develop the ZPM attitude trajectory for ISS, a general rotational-state-transition problem is solved. The objective is to maneuver the spacecraft between specified initial and final attitude, rate, and CMG momentum values while constraining the peak CMG momentum and torque magnitudes to remain below saturation levels. To simplify formulation of the rotational-state-transition problem, we assume that the spacecraft can be treated as a single rigid body. Using a quadratic cost function to minimize the control torque, one ZPM formulation is given by

$$\min \int_{t_0}^{t_f} \|u\|^2 dt, \tag{7}$$

such that, for $t_0 \leq t \leq t_f$, the system states satisfy the rate dynamics [7]

$$\dot{\omega} = J^{-1}[-\omega \times (J\omega + \mathrm{H}_{\mathrm{CMG}}) - \dot{\mathrm{H}}_{\mathrm{CMG}} + T_{\mathrm{grav}} + T_{\mathrm{aero}}], \tag{8}$$

with the attitude kinematics represented by a quaternion parameterization [7]

$$\dot{q} = \frac{1}{2}\begin{bmatrix} -q_2 & -q_3 & -q_4 \\ q_1 & -q_4 & q_3 \\ q_4 & q_1 & -q_2 \\ -q_3 & q_2 & q_1 \end{bmatrix} \tilde{\omega}, \tag{9}$$

where q and $\tilde{\omega} = \omega - \omega_{\mathrm{LVLH}}$ are the ISS attitude and rate relative to the local vertical local horizontal (LVLH) reference frame rotating at ω_{LVLH} with the positive x-axis pointing in the direction of the ISS velocity vector and the positive z-axis pointing toward the center of the Earth, the CMG momentum dynamics

$$\dot{\mathrm{H}}_{\mathrm{CMG}} = u - \omega \times \mathrm{H}_{\mathrm{CMG}}, \tag{10}$$

Since the ISS is in low-Earth orbit at an altitude of 300 km, it experiences environmental disturbances that depend on attitude.

the quaternion, momentum, and torque path constraints

$$\|q\| = 1, \quad \|\mathrm{H}_{\mathrm{CMG}}\| \le \mathrm{H}_{\max}, \quad \|\dot{\mathrm{H}}_{\mathrm{CMG}}\| \le \dot{\mathrm{H}}_{\max}, \tag{11}$$

and the boundary conditions

$$\begin{aligned} q(t_0) &= q_0, \quad \omega(t_0) = \omega_0, \quad \mathrm{H}_{\mathrm{CMG}}(t_0) = \mathrm{H}_0, \\ q(t_f) &= q_f, \quad \omega(t_f) = \omega_f, \quad \mathrm{H}_{\mathrm{CMG}}(t_f) = \mathrm{H}_f. \end{aligned} \tag{12}$$

The vehicle inertia, final time, initial and final states, as well as momentum and torque path constraint bounds are user-specified parameters. Because the trajectory depends on accurate knowledge of the system parameters and initial conditions, the saturation constraints must include a margin of safety to account for deviation from expected values. The final time and CMG momentum bound must be chosen carefully to ensure the largest possible CMG momentum margin. In general, as the maneuver time decreases, the peak CMG momentum needed to complete the maneuver increases. An iterative process is used to select the final time to achieve a desirable momentum margin of safety.

NUMERICAL SOLUTION OF OPTIMAL TRAJECTORY

Since an analytical solution is not available for (7)–(12), numerical methods are used to determine the ZPM. In

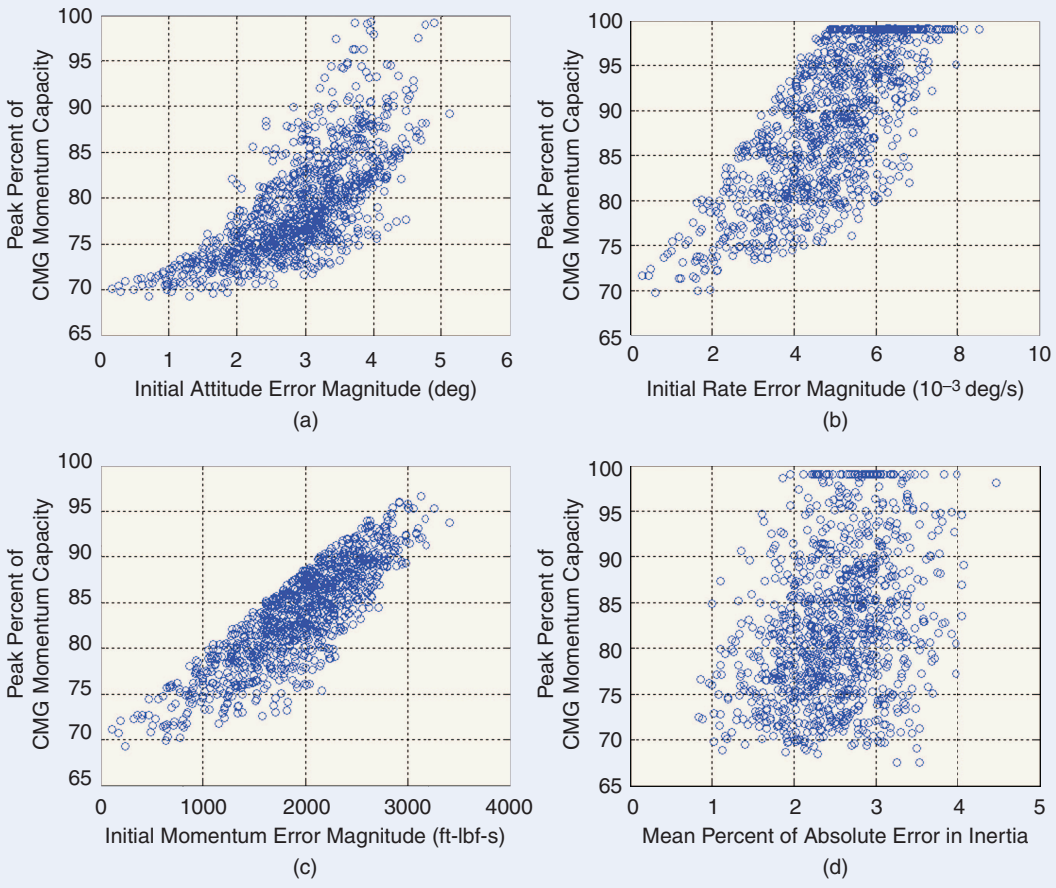

FIGURE 6 Simulated robustness of a 90° zero-propellant maneuver trajectory to errors in initial conditions and inertia. Control moment gyroscope (CMG) saturation for this trajectory can occur for either initial-condition error magnitudes greater than about (a) 3.5° for attitude, (b) 0.0045 deg/s for rate, and (c) 3000 ft-lbf-s for CMG momentum, or (d) an average error in the components of the inertia matrix of 2%. An alternative trajectory is required if the errors are expected to be in these ranges.

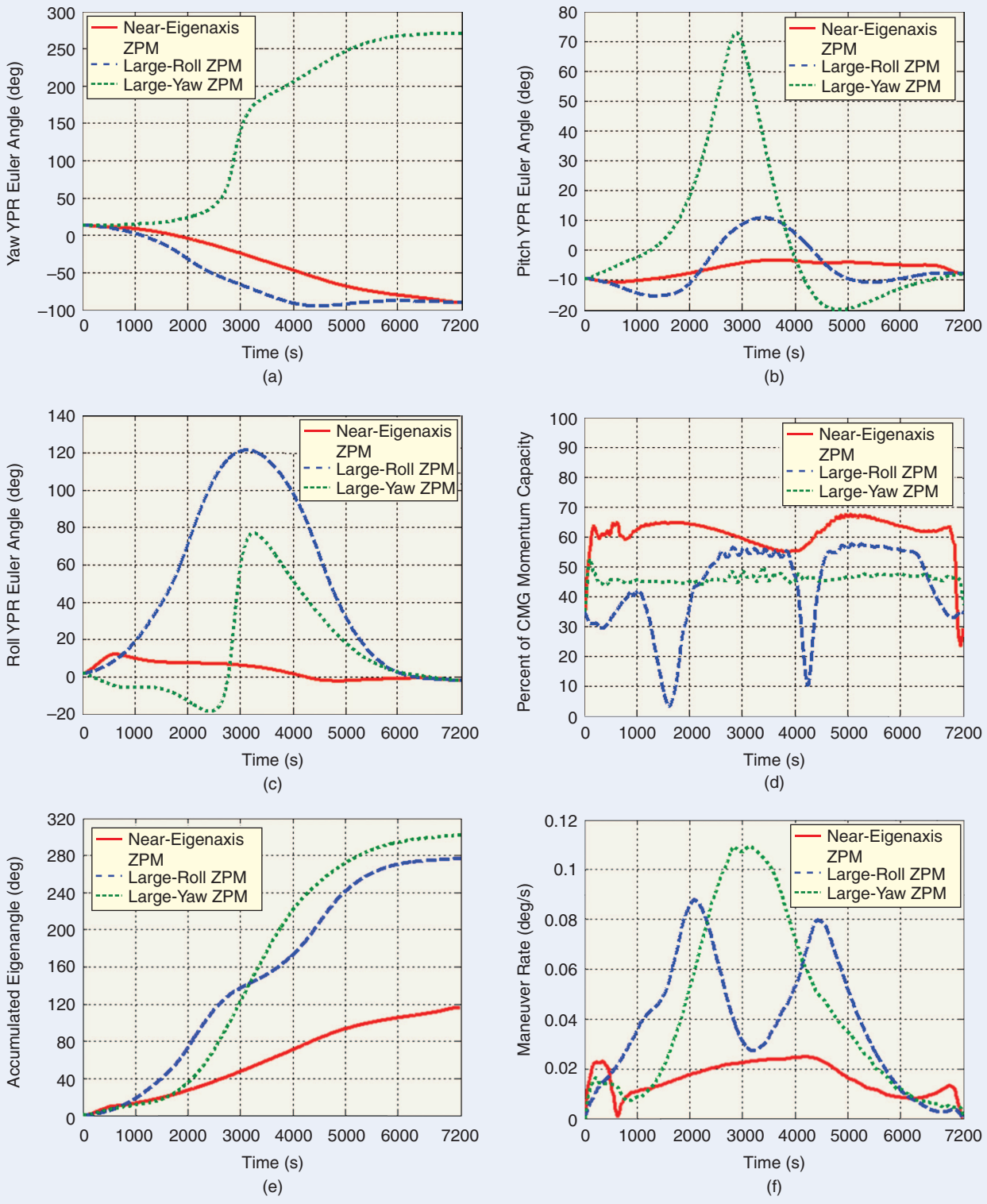

FIGURE 7 Simulated trajectories computed using pseudospectral optimal control. Multiple solutions are found for a 90° zero-propellant maneuver (ZPM) with three control moment gyroscopes (CMGs). In (a)–(c), the International Space Station attitude is relative to the local vertical local horizontal frame expressed by a yaw-pitch-roll Euler-angle sequence. CMG momentum usage, accumulated eigenangle, and maneuver rate are shown in (d), (e), and (f), respectively. The trajectories are discovered by using a collection of initial guesses. Surprisingly, the large-yaw ZPM (green), which rotates backwards by 270°, has the lowest momentum peak. The near-eigenaxis trajectory (red) was delivered to Mission Control Center on November 1 since it did not require additional thermal analysis.

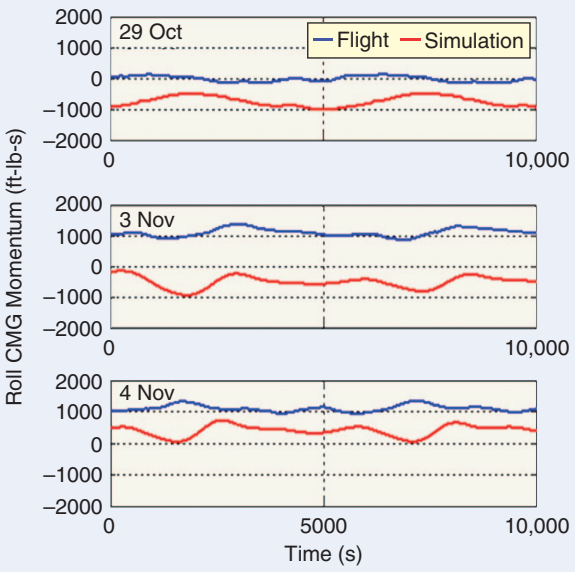

FIGURE 8 A comparison of control moment gyroscope (CMG) roll-axis momentum. Prior to the first zero-propellant maneuver, the CMG momentum from flight (blue) was compared to simulation (red). On October 29, 2006, the flight telemetry matched simulation within 1000 ft-lbf-s. However, after payload translation, the flight telemetry momentum increased by 1000 ft-lbf-s, and the difference between flight and simulation almost doubled as seen on November 3, 2006. After updating the mass properties to account for payload translation, the simulation results for November 4 were within 1000 ft-lbf-s of flight data and consistent with previous observations.

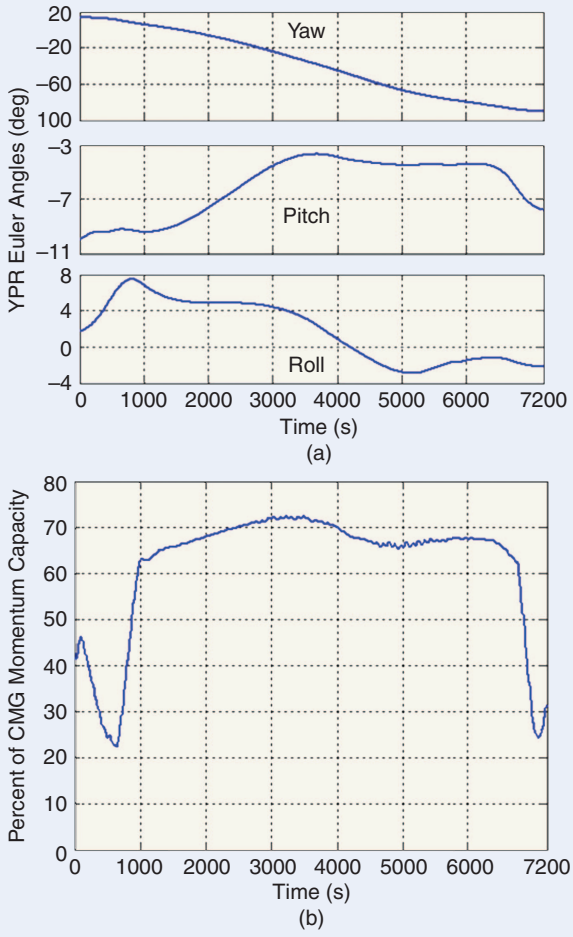

FIGURE 9 Simulation of the final solution for the 90° zero-propellant maneuver. The International Space Station attitude shown in (a) is relative to the local vertical local horizontal frame expressed by a yaw-pitch-roll Euler-angle sequence. By accounting for the translation of the mobile transporter and the Space Station Remote Manipulator System, the trajectory does not exceed 72% of peak momentum capacity.

particular, we use the commercial software package DIDO [18], which implements the Legendre pseudospectral optimization method within the Matlab environment. For further information, see "Pseudospectral Dynamic Optimization." To implement this approach, the user must choose objective and constraint functions, provide an initial guess to the solver, and scale the variables.

To solve the dynamic optimization problem, an initial guess for the trajectory is usually needed. Although DIDO does not require an initial guess [19], a user-provided guess can enhance its convergence properties. Since the optimal trajectory is not known a priori, various initial paths may need to be provided to the solver before a solution is obtained. For ZPM, the typical initial guess is the eigenaxis trajectory. Because the optimization problem does not necessarily have a unique solution, different initial trajectories can be used to discover new solutions. Furthermore, the optimization problem can be posed in different ways, and the particular formulation can affect the performance of the solver. For example, a constraint can be imposed directly or instead be included in the cost function.

Once the dynamic optimization problem has been formulated, scaling the problem involves transforming the states to normalize their magnitude and thus avoid ill-conditioning. Typically, either a dynamic optimization problem cannot be solved without some form of scaling, or it takes a long time to obtain a solution. For best results, some iteration may be necessary to determine good scaling factors. In the case of ZPM, the dynamic optimization problem is initially solved for various scaling factors and evaluated for feasibility of solution. The best performing scaling is then selected and used to develop the flight trajectories.

Robustness of Optimal Trajectory

Since the nonpropulsive maneuver is an open-loop trajectory computed based on initial states (attitude, rate, CMG momentum) and ISS dynamics (including inertia, surface area, and atmospheric density), the peak CMG momentum magnitude along the trajectory depends on how accurately these quantities are known. Before the optimal trajectory

can be used, it is thus necessary to evaluate its sensitivity. Robustness analysis is performed using simulations to determine the range of uncertainty in initial states and ISS dynamics for which the maneuver can be completed without CMG saturation. The simulation includes articulating multibody dynamics, high-fidelity gravitational and atmospheric models, and the actual ISS flight software. If necessary, the optimization process is repeated until the required level of robustness is achieved.

As an example, robustness results for the 90° ZPM flight trajectory are shown in Figure 6. To assess sensitivity to error sources such as initial conditions, Monte Carlo simulations are performed with only a single variable perturbed at a time. Since interaction effects between variables are excluded, the effect of initial attitude, initial rate, initial momentum, and inertia are each considered separately. Each variable is sampled from a uniform distribution centered about the nominal value. This procedure shows that the momentum along the trajectory does not saturate if the independent initial errors for attitude, rate, momentum, and inertia are less than approximately 3.5°, 0.0045°/s, 3000 ft-lbf-s, and 2%, respectively. If the flight conditions are outside these uncertainty ranges, the trajectory needs to be redesigned.

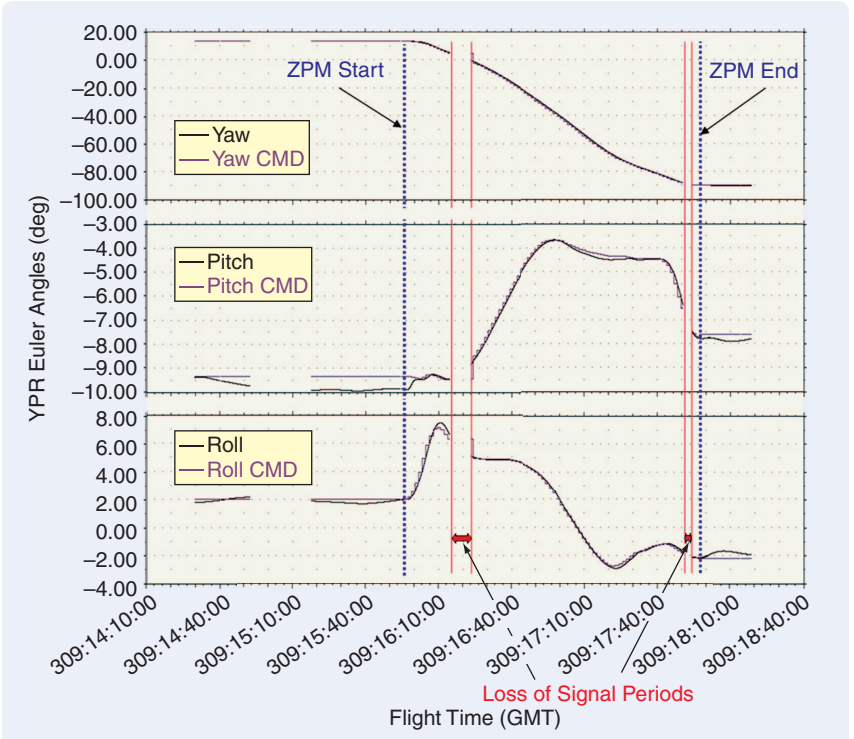

FIGURE 10 The 90° zero-propellant maneuver flight attitude telemetry. The International Space Station commanded attitude relative to the local vertical local horizontal frame expressed by a yaw-pitch-roll Euler-angle sequence is shown in purple, while the actual attitude is in black. The commands were uploaded to the station prior to the maneuver and were issued every 90 s. While the state telemetry was unavailable to the ground during loss of signal periods (indicated in red), all commands were executed as planned.

TIMELINE FOR 90° ZPM DEMONSTRATION

To illustrate the systems engineering process for ZPM, we present the timeline associated with the first ZPM, the 90° ISS reorientation on November 5, 2006. The approach consists of four steps: a) calibrate simulation models against flight data, b) design the ZPM trajectory for nominal system parameters, c) verify the design and evaluate its robustness in simulation, and d) repeat the process as necessary. The design process was started in the summer of 2006 assuming four operational CMGs. The design objective was to complete the maneuver in a reasonable time period while providing a margin of safety by limiting the peak CMG momentum magnitude during the trajectory. The ZPM problem was solved for various maneuver times until a peak momentum below 70% of CMG capacity was achieved. Although increasing the maneuver time led to lower overall peak momentum solutions, the maximum maneuver duration was limited by planned ISS operations. Based on environmental predictions for November, expected ISS initial conditions and operational mode, a trajectory was designed that completed the maneuver in 6000 s,

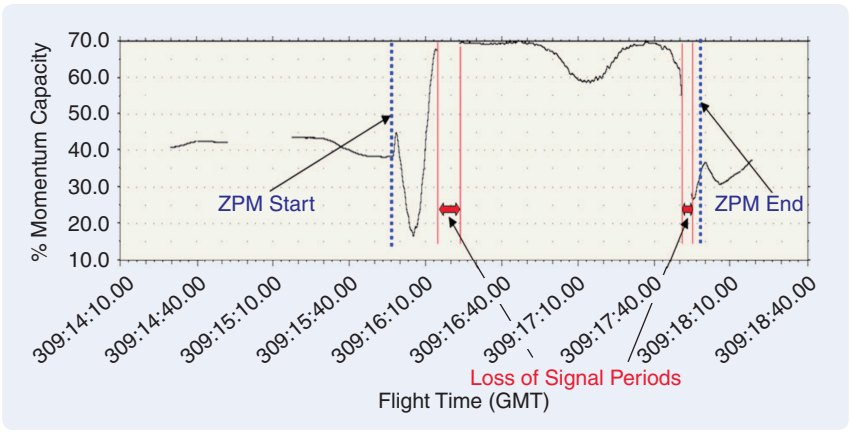

FIGURE 11 The 90° zero-propellant-maneuver flight momentum-capacity telemetry. The maneuver is completed using less than 70% of the control moment gyroscope momentum capacity.

a little over one orbit, with peak momentum less than 65% capacity. This trajectory was delivered to the Mission Control Center (MCC) at NASA Johnson Space Center in September 2006.

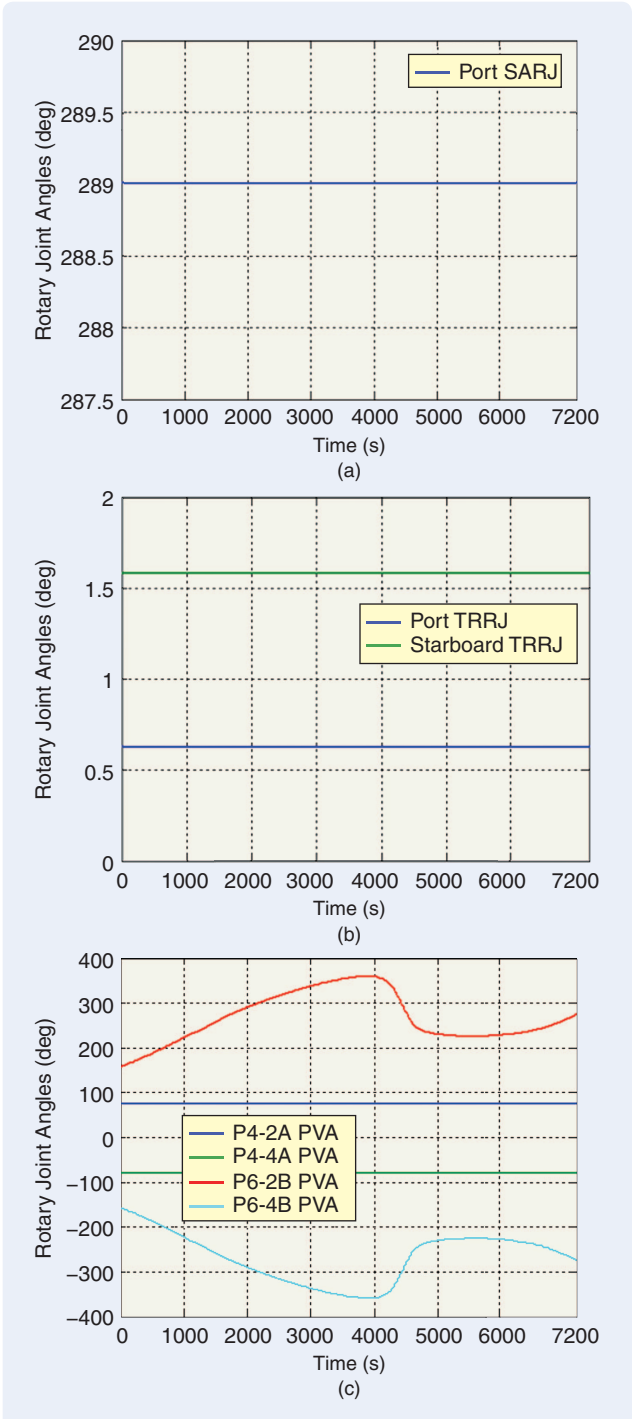

FIGURE 12 The 90° zero-propellant maneuver (ZPM) flight rotary joint angle telemetry. The (a) solar array rotary joint (SARJ) and (b) TRRJs were fixed as were (c) the P4 solar arrays. The (c) P6-2B and P6-4B solar arrays were rotating during the ZPM. The FGB and SM solar arrays (not shown) were also rotating.

Before delivery, however, one of the CMGs showed signs of excessive wheel vibration, and NASA made the decision on October 10 to shut it down. With the loss of 25% CMG capacity, the momentum peak now reached 87% of three-CMG capacity for the design delivered in September 2006. Since the safety margin was substantially reduced, the trajectory was redesigned. To achieve acceptable margins, the maneuver time was increased to 7200 s, and three different trajectories, shown in Figure 7, were generated. These solutions are identified based on their prominent attitude properties when compared to the other two solutions, a) the first solution was labeled near-eigenaxis since the attitude profile most closely

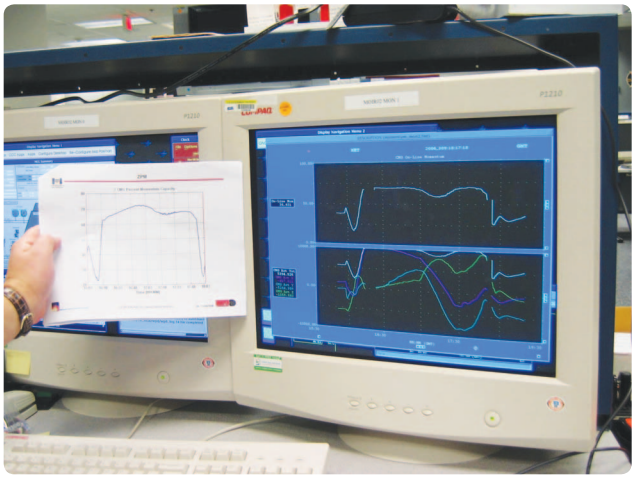

FIGURE 13 Photograph taken in Mission Evaluation Room on November 5, 2006. The predicted 90° zero-propellant-maneuver momentum performance, which is less than 72% of total control moment gyroscope capacity, is compared to flight telemetry (top plot on screen), which was less than 70% capacity.

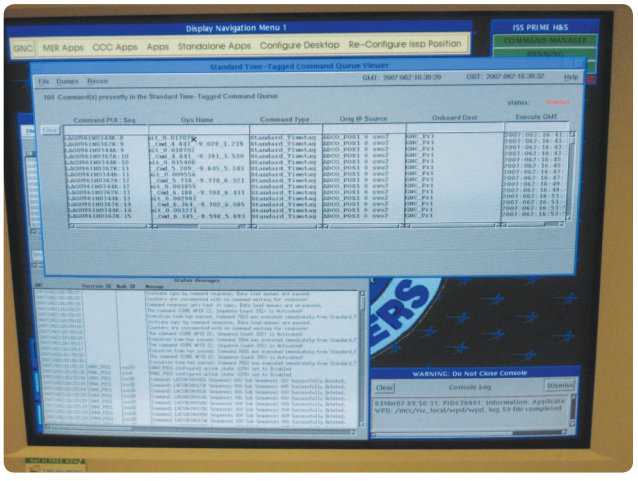

FIGURE 14 Photograph taken in Mission Evaluation Room on March 3, 2007. The 180° zero-propellant-maneuver (ZPM) time-tagged commands are shown during maneuver execution. Each ZPM is allocated 160 commands consisting of 80 attitude and maneuver rate pairs to be uploaded to the International Space Station flight computer before the maneuver starts.

resembles an eigenaxis trajectory, b) the second solution was labeled large-roll since its attitude profile has the largest roll-angle excursion, and c) the third solution was labeled large-yaw since its attitude profile has the largest yaw-angle excursion. These results were obtained by using different initial guesses [20]. It is seen in Figure 7(d) that the lowest peak momentum, about 53% of capacity, was obtained with the large-yaw maneuver that rotates the ISS backwards by 270°. This trajectory has the largest accumulated angular distance of approximately 300° [Figure 7(e)]. However, since thermal analysis had already been performed for an eigenaxis maneuver, NASA selected the near-eigenaxis solution because the attitude excursions remained within acceptable thermal analysis bounds. On November 1, this solution was delivered to MCC for upload to ISS.

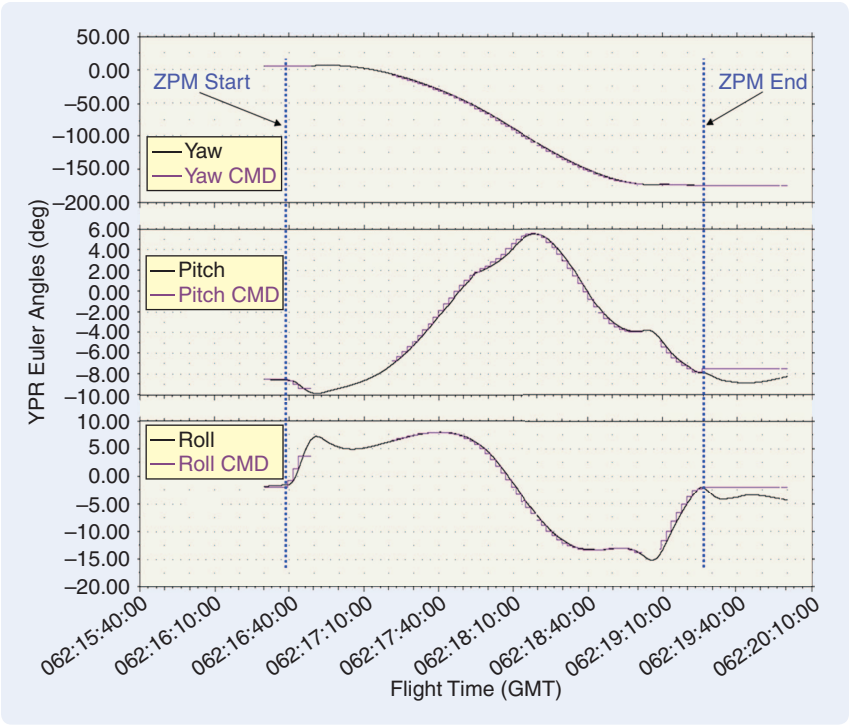

FIGURE 15 The 180° zero-propellant maneuver flight attitude telemetry. The ISS commanded attitude relative to the local vertical local horizontal frame expressed by a yaw-pitch-roll Euler-angle sequence is shown in purple, while the actual attitude is in black. The commands were uploaded to the station prior to the maneuver and were issued every 125 s.

These plans were affected, however, by ISS operations on November 3, when a 10,000-lbm mass payload was translated 80 ft. This payload, which consisted of the Space Station Remote Manipulator System atop the Mobile Transporter, was moved as a test of an operational scenario for an upcoming assembly operation. This motion altered both the ISS rotational states and its mass properties. From flight telemetry, the ISS pitch attitude changed by 1°, while the roll CMG momentum change was 10% of capacity. On the morning of November 4, the change in ISS inertia due to payload motion was calculated to be greater than 5%. The robustness results for the existing trajectory with only the new initial conditions indicated a nearly acceptable peak of 80% momentum capacity. However, the change in inertia was large enough that the potential for momentum saturation would be high if the trajectory were not redesigned. But before redesigning the trajectory, the new mass properties had to be calibrated with flight data. This calibration was accomplished by comparing simulation to flight data.

As part of the design process and to gain confidence, simulation predictions were calibrated against flight data on a regular basis. This process could now be used to verify the new mass properties. Comparisons were carried out for multiple time frames as shown in Figure 8. Leading up to the demonstration, a difference between flight and simulation of around 1000 ft-lbf-s had been consistently observed in the roll-axis momentum, as seen on October 29. Although this difference is attributed to simulation fidelity, consistency is considered more valuable than absolute accuracy since it increases confidence in predictions [21]. The November 3 flight telemetry showed a CMG roll momentum difference from simulation of about 2000 ft-lbf-s, which was consistent with a change in the ISS configuration. After adjusting the mass properties to account for the payload translation, comparison with November 4 flight data showed a signature that was similar

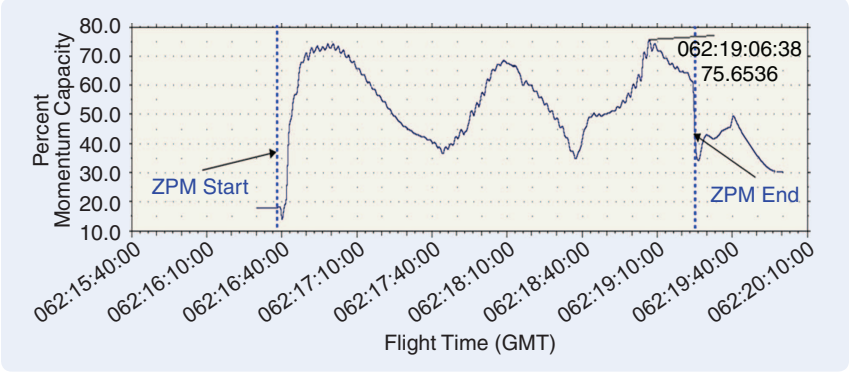

FIGURE 16 The 180° zero-propellant-maneuver flight momentum-capacity telemetry. The maneuver is completed using less than 76% of the momentum capacity.

to the October 29 flight data, a difference of 1000 ft-lbf-s, thereby providing confidence in the new mass property estimate. When the existing trajectory was simulated with the new mass properties, the peak momentum reached 88% of capacity, which did not provide enough safety margin.

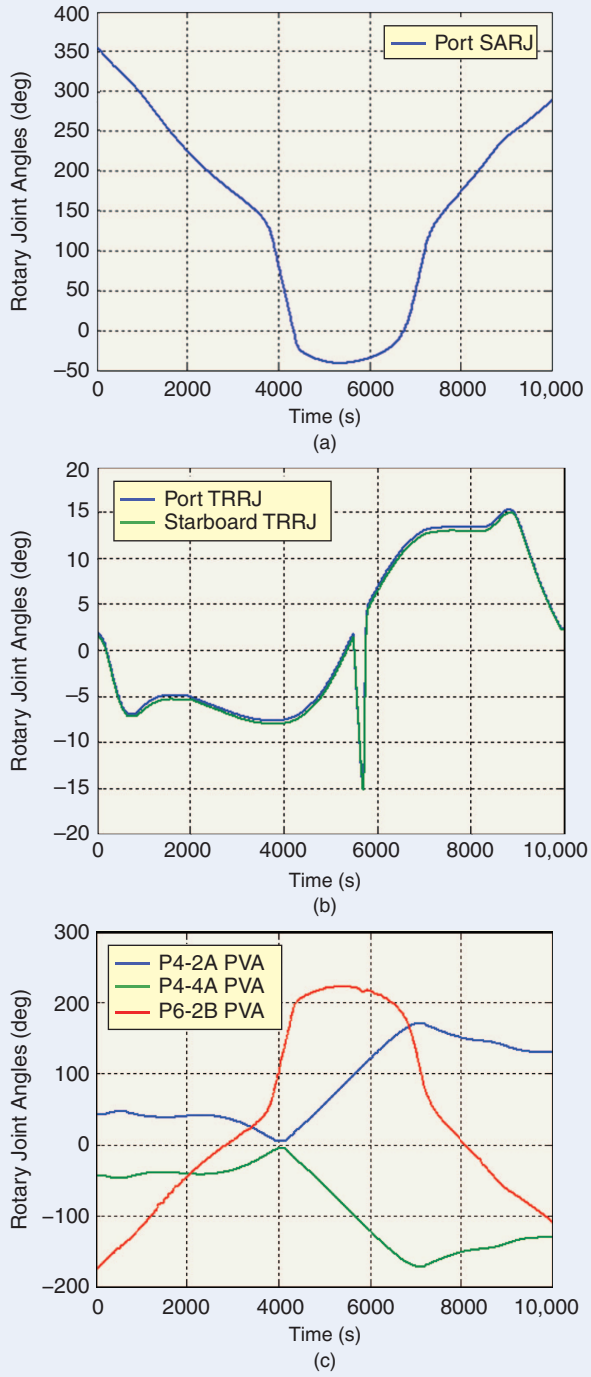

FIGURE 17 The 180° zero-propellant maneuver (ZPM) flight rotary joint angle telemetry. The (a) solar array rotary joint (SARJ), (b) TRRJs, (c) P4 and P6 solar arrays, and FGB and SM solar arrays (not shown) were rotating during the ZPM.

Once again, the trajectory had to be redesigned using the new initial conditions and inertia.

In the afternoon of November 4, to speed up the design process, various formulations of the ZPM problem with different initial guesses were solved on multiple computers in parallel, followed by Monte Carlo sensitivity analysis of the selected solution. The final ZPM, shown in Figure 9, used 72% of momentum capacity and was delivered to MCC on the night of November 4. Between the summer of 2006 and the delivery of this final ZPM trajectory, an estimated 1000 versions of the dynamic optimization problem were solved to accommodate parameter updates and operational changes.

ZPM Flight Demonstration Results

Once the final trajectory was delivered to MCC, it was converted into a sequence of time-tagged command packets

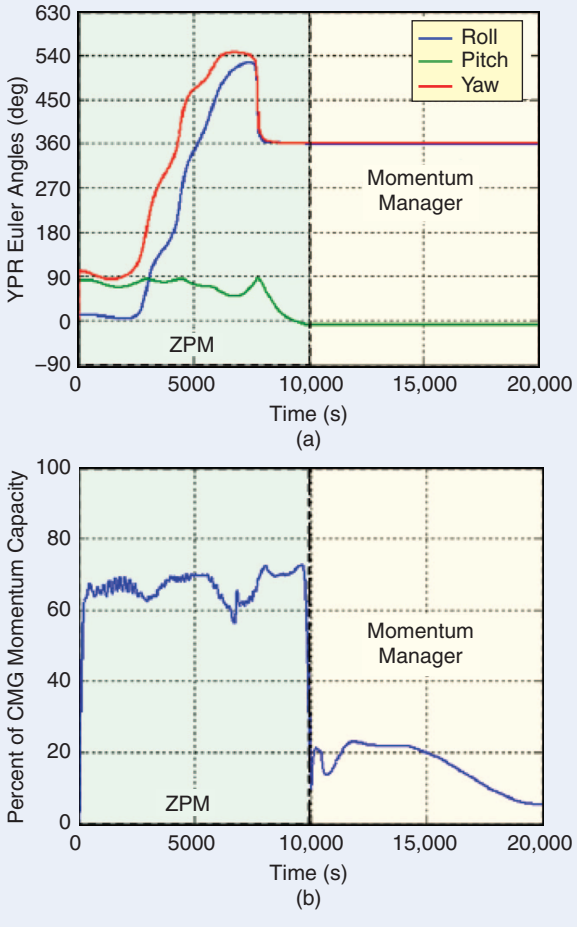

FIGURE 18 Zero-propellant maneuver (ZPM) (a) attitude and (b) momentum for International Space Station (ISS) rescue. A simulated transition from a stable attitude to momentum manager is shown. The ISS attitude is relative to the local vertical local horizontal frame expressed by a yaw-pitch-roll Euler-angle sequence. The peak momentum during the maneuver remains below 75% of capacity, and the momentum manager activation is successful.

with the commands designated to start at specified Greenwich mean times. The operational scenario started in momentum manager control mode, which is used for long-term attitude hold. Then the CMG PD controller was activated to perform the 90° maneuver by following the ZPM commands. Once the maneuver was complete, control transitioned back to momentum manager at the new attitude. Since the flight computer command buffer is limited, 160 slots were allocated to ZPM, which consisted of 80 command pairs, each composed of an attitude relative to the LVLH frame and a scalar maneuver rate. The complete set of commands was uploaded to the ISS during the night of November 4, 2006. Since the trajectory was defined in terms of commands to the onboard PD controller, no flight software modifications were required for onboard implementation. Because the flight software could use different maneuver rates between attitude commands, the ZPM trajectory was implemented by commanding 80 different constant-rate eigenaxis rotations.

For the 90° ZPM from an initial attitude of $[13\ -9\ 2]$ degrees to a final attitude of $[-90\ -8\ -2]$ degrees relative

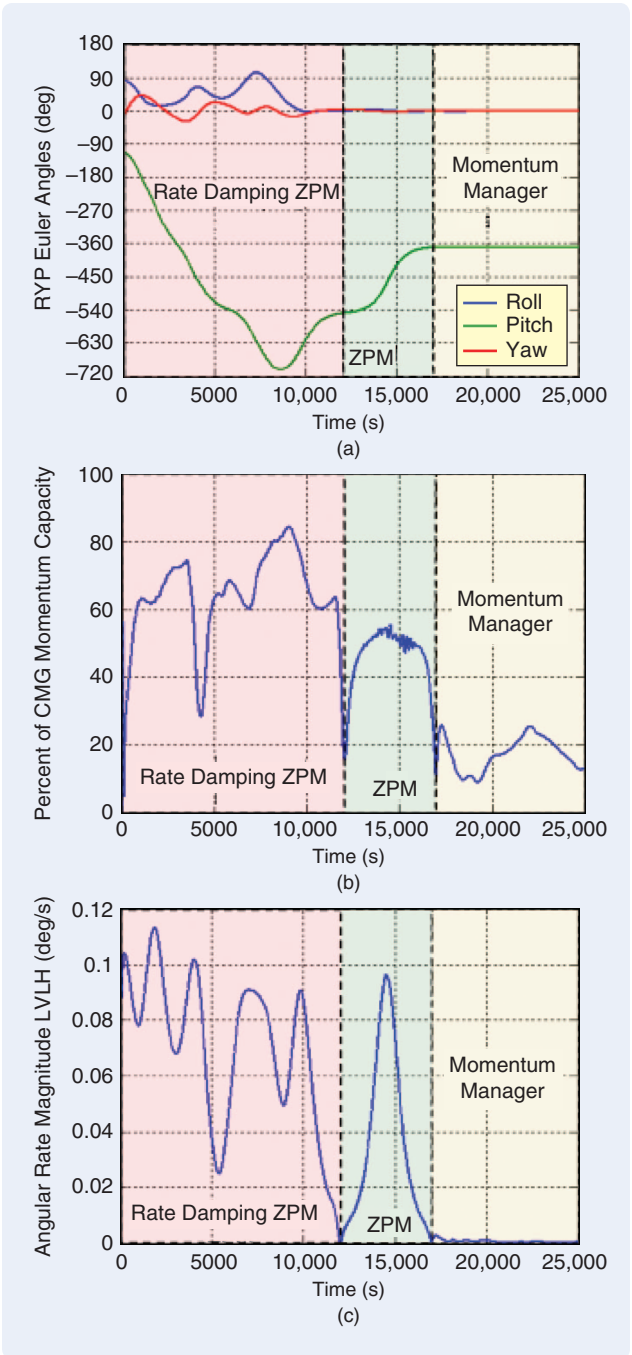

FIGURE 19 Simulation of catching a tumbling International Space Station (ISS) with zero-propellant maneuver (ZPM). The first ZPM, which starts with an ISS rate of $[0.085\ -0.043\ -0.023]$ deg/s relative to the local vertical local horizontal (LVLH) frame, damps the rate as shown in (c), while the second ZPM performs a complete rotational state transition, including (a) attitude and (b) momentum, to hand off to the momentum manager. The ISS attitude in (a) is relative to the LVLH frame expressed by a roll-yaw-pitch Euler-angle sequence.

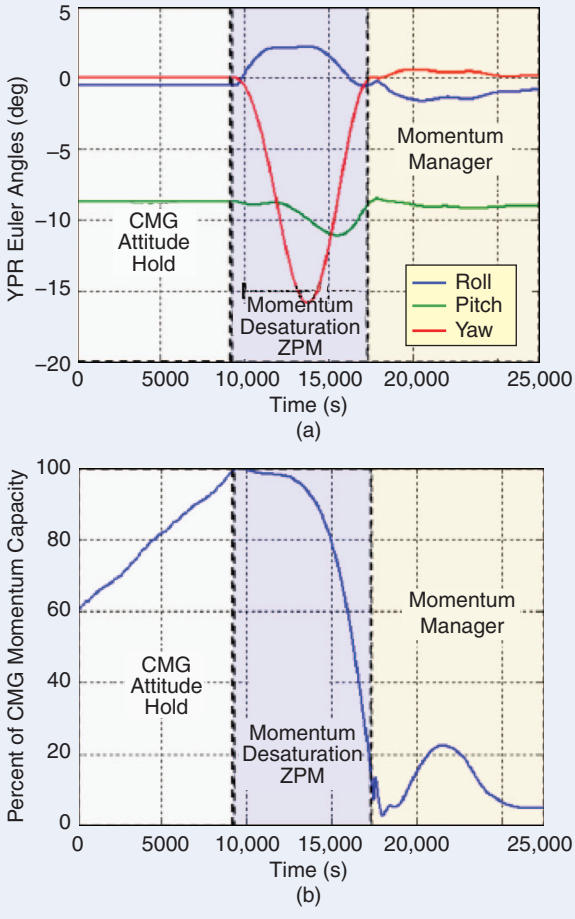

FIGURE 20 Simulation of zero-propellant maneuver (ZPM) attitude control with momentum-saturated control moment gyroscopes (CMGs). When the CMGs reach momentum saturation, attitude control is not truly lost because the saturation is directional. Thus with (a) the special attitude trajectory, (b) nonpropulsive desaturation of 90% of momentum capacity is achieved in 8000 s to transfer control to the momentum manager. The ISS attitude in (a) is relative to the local vertical local horizontal frame expressed by a yaw-pitch-roll Euler-angle sequence.

A rate-damping ZPM arrests a tumbling ISS, whereas an attitude-targeting ZPM returns the ISS to its operating attitude.

to LVLH (yaw-pitch-roll order and sequence), the ISS configuration is shown in Figure 1(a). The flight telemetry for commanded and actual attitudes, percent of CMG momentum capacity used, and rotary joint motion are shown in figures 10, 11, and 12, respectively. The ISS state telemetry signal was lost during two periods, namely, at the beginning and at the end of the maneuver when the momentum was changing rapidly. The maneuver was completed in 2 h with a new command issued every 90 s. The peak momentum magnitude remained below 70% of CMG capacity, while the predicted peak was 72%. Figure 11 shows that 40% momentum desaturation of CMG capacity was performed by the CMGs while rotating the ISS. A comparison of the peak momentum profile is shown in Figure 13. After the maneuver was completed, momentum manager startup was successful.

Following the success of the first ZPM, a 180° maneuver from an initial attitude of [5 −8.5 −2] degrees to a final attitude of [−175 −8 −2] degrees relative to LVLH (yaw-pitch-roll order and sequence) was performed on March 3, 2007 for the ISS configuration shown in Figure 1(b). In this case, a significant portion, approximately 10% of the ISS mass, was in motion due to the solar array rotary joint tracking the sun. The uploaded time-tagged ZPM commands are shown in Figure 14. The maneuver completed in 2 h, 47 min with a new command issued every 125 s. The flight telemetry for commanded and actual attitudes, percent of CMG momentum capacity used, and rotary joint motion are shown in figures 15, 16, and 17. The maneuver was completed with peak momentum magnitude reaching 76% of CMG capacity. The results show that, after the maneuver was completed, transition to momentum manager control was successful.

ADDITIONAL CMG CAPABILITIES USING ZPM GUIDANCE

After the flight demonstrations, NASA authorized the use of ZPM for ISS operations. Although it was expected that ZPM would be used for future large-angle maneuvers, a few months later an unexpected event provided an opportunity to reveal other potential capabilities of ZPM optimal guidance for CMGs. This development was the failure of the ISS Russian guidance, navigation, and control computers while the Orbiter was mated to the ISS during Shuttle mission STS-117 in June 2007 [22]. The nominal undocking procedure was to use thruster attitude control first to maneuver the ISS from the undock attitude to the unmated long-term attitude and then to trim the rate errors to less than 0.001°/s [23], required by the momentum manager controller for successful startup. However, the computer failure caused the loss of closed-loop attitude control capability using thrusters. If the ISS could not regain attitude control after the Orbiter undocked, it would tumble out of control since the Orbiter undocking attitude is dynamically unstable. In this circumstance, the ISS would have to be abandoned with the crew escaping using the Soyuz capsule. Hence, the core issue was how to undock so that momentum manager control could be successfully activated.

Several rescue plans based on ZPM were developed before the scheduled date of Orbiter undocking. Because the unmated ISS long-term attitude is unstable, the operational procedure with the highest probability of success was to maneuver the mated assembly with the Orbiter thrusters to a safe-harbor stable unmated attitude. After the Orbiter departs, the ISS could remain at this attitude without active control. Subsequently, a ZPM could be used to maneuver the ISS back to the desired attitude. Then the momentum manager controller would be activated to maintain orientation [5]. Figure 18 shows an example of a ZPM that maneuvers the ISS from the safe-harbor attitude to the attitude target for momentum manager control in 10,000 s followed by successful activation of the momentum manager. The peak momentum during the ZPM remained less than 75% of capacity.

Alternative scenarios were also considered. The most challenging scenario would be to arrest a tumbling ISS using a ZPM. In this case, a two-phase ZPM rescue was envisioned. A rate-damping ZPM arrests a tumbling ISS while an attitude-targeting ZPM returns the ISS to its operating attitude. In the first phase, a ZPM would be developed to reduce the rate error relative to LVLH to zero. At the end of this phase, the ISS may not be in the desired orientation for momentum manager control. For this reason, a second ZPM would be designed to transition the ISS to the attitude, rate, and CMG momentum needed for handover to momentum manager control. Figure 19 shows an example with the two ZPMs that damp a rate error of 0.1°/s in 12,000 s and then maneuver to the attitude target for momentum manager control in 5000 s. It is seen that momentum manager startup is successful, and peak momentum during both ZPMs remains less than 85% of capacity.

In the final scenario considered, the CMG PD controller would maintain attitude after undock until the CMGs saturated, whereupon a ZPM could be used to desaturate the momentum so that CMGs can regain attitude control.

The goal of the ZPM desaturation trajectory is to reach a desired attitude while minimizing the final total momentum of the CMGs. As long as the three-axis saturated momentum state is known, a ZPM can be designed to desaturate the CMGs and target the momentum manager initial conditions. For the example shown in Figure 20, a ZPM is used to desaturate 90% of CMG capacity in 8000 s and successfully hand off to the momentum manager.

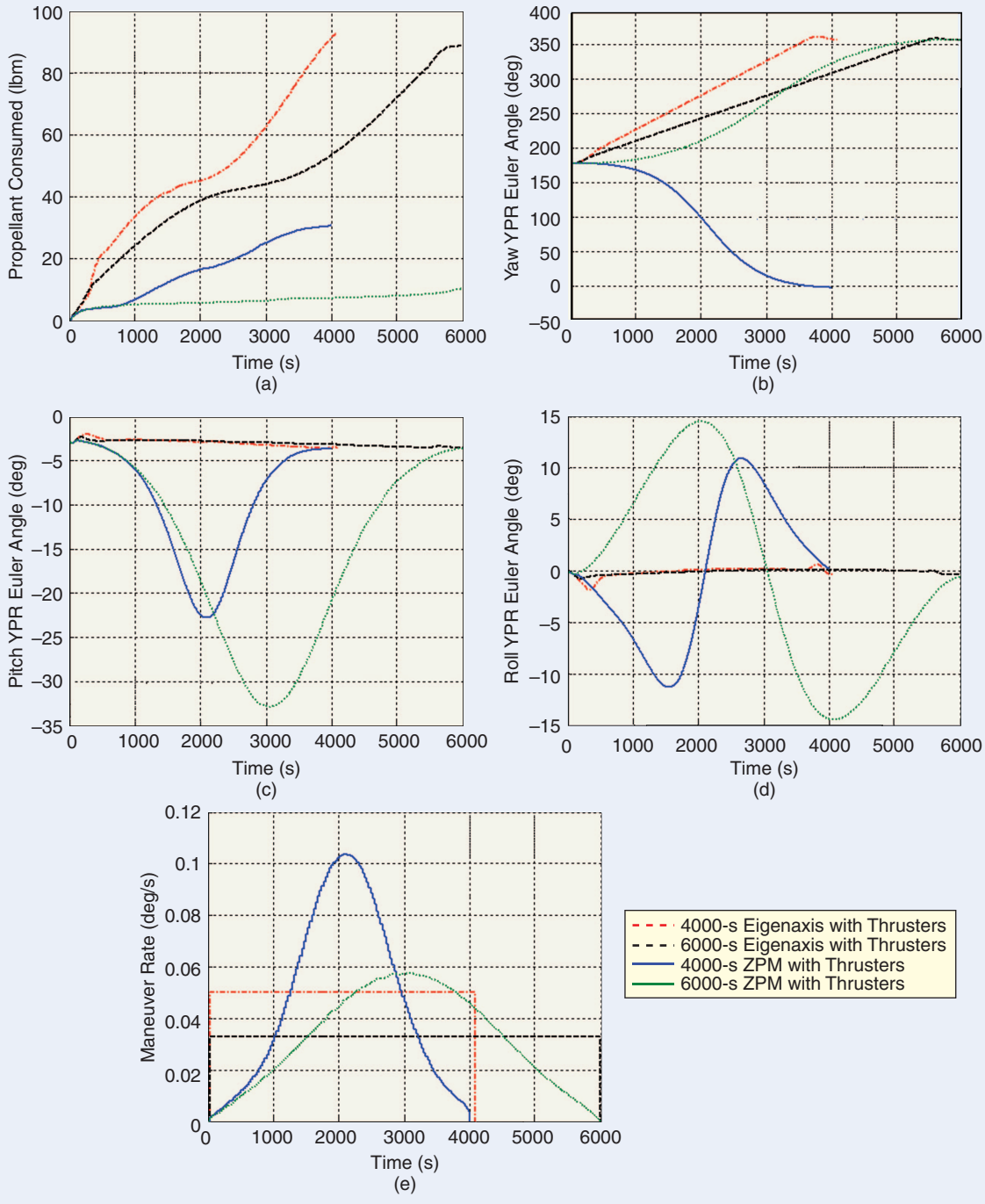

FIGURE 21 Simulated propulsive maneuvers using eigenaxis and zero-propellant maneuver (ZPM) trajectories. The 180° yaw maneuvers with durations 4000 s and 6000 s were performed with thrusters in simulation using constant-rate eigenaxis trajectories and ZPM trajectories. The ZPM trajectory saves 67% propellant over the constant-rate eigenaxis trajectory for a maneuver time of 4000 s and saves nearly 90% if the maneuver time is extended (a). The ISS attitude shown in (b)–(d) is relative to the local vertical local horizontal frame expressed by a yaw-pitch-roll Euler-angle sequence. Note that the two ZPMs rotate in opposite directions about yaw to arrive at the same attitude (−3° = 357°). The maneuver rates are given in (e).

For thruster-actuated maneuvers, a ZPM trajectory can still be used to reduce propellant consumption.

Fortunately, a day before the scheduled Orbiter undocking, the Russian computers were successfully brought online, and automatic thruster control capability was restored. Thus the above ZPMs were not needed, and Orbiter undocking was performed on schedule.

ZPM GUIDANCE FOR THRUSTERS

For thruster-actuated maneuvers, a ZPM trajectory can still be used to reduce propellant consumption. The decreased propellant consumption is due to the ZPM-reduced peak momentum needed from the actuators to complete the maneuver. Using thrusters as torque actuators, the momentum provided by thrusters is proportional to thruster on-times. By reducing the peak momentum, we reduce the change in momentum needed to start and stop the maneuver, thereby reducing the thruster on-times. Unlike the CMG case, propellant savings can be achieved even without increasing the time to complete the maneuver.

Using ISS as an example, we can compare the efficiency of this method. Fortunately, the control system architecture for a ZPM-driven thruster rotation exists on the ISS and is called United States thruster only (USTO) control mode [24]. USTO was originally developed to provide ISS-Orbiter stack attitude control capability for a contingency tile-repair scenario, where the Orbiter is maneuvered using its robotic manipulator relative to the ISS. Since 2005 USTO has been used for nominal ISS operations. By using a pulse-width modulator, the CMG attitude hold PD controller torque command is converted to an equivalent change in angular momentum command, which is then used to compute thruster on-times. A minimum-momentum threshold is used to keep the thrusters from firing for very short periods.

The implementation of a ZPM-driven thruster rotation is identical to the CMG implementation.

Figure 21 shows simulation results from an illustrative 180° yaw maneuver performed with thrusters. ZPM trajectories designed to perform the same 180° yaw maneuver in 4000 s and 6000 s are compared to constant-rate eigenaxis rotations. The 4000-s eigenaxis rotation uses a maneuver rate of 0.05°/s, while the 6000-s eigenaxis rotation uses a maneuver rate of 0.033°/s. The eigenaxis trajectory uses three times as much propellant as the ZPM trajectory for the shorter maneuver time. Whereas the longer time eigenaxis trajectory does not provide much reduction in propellant consumption over its shorter time counterpart, increasing the maneuver time for ZPM significantly decreases propellant usage. The 6000-s eigenaxis trajectory uses nine times as much propellant as the 6000-s ZPM. The propellant savings are representative of what can be expected from thruster-commanded ZPM trajectories.

CONCLUSIONS

In this article we have shown that dynamic optimization can be used to discover new trajectories, such as ZPMs, which enable new capabilities. By exploiting the physics of the problem, we developed optimal guidance trajectories that desaturate accumulated angular momentum using momentum-storage devices instead of thrusters. Using ZPM, the need for thrusters as backup to momentum-storage actuators for rotational control is minimized or eliminated. For the ISS, optimal trajectories were used to shape the command to a standard feedback controller. The flight success of maneuvering the Space Station demonstrates that dynamic optimization methods provide a framework for solving challenging guidance and control problems for highly nonlinear systems in which computational optimization is treated as a first principle in control design that works in harmony with a feedback architecture.

ACKNOWLEDGMENTS

The thesis [25] was joint research between The Charles Stark Draper Laboratory, Inc., under NASA contract NNJ06HC37C and Prof. Yin Zhang of the Computational and Applied Mathematics department at Rice University. The last author gratefully acknowledges partial funding provided by NASA Glenn Research Center to perform a preliminary ZPM analysis using pseudospectral dynamic optimization.

AUTHOR INFORMATION

Nazareth S. Bedrossian (naz@draper.com) is group leader for manned space systems and a distinguished member of the technical staff at the Charles Stark Draper Laboratory. He leads design and flight-readiness certification for Space Shuttle, Space Station, and Ares-I flight control systems. Since 1992, he has been at NASA Johnson Space Center and has also worked with Canadian and Japanese Space Agencies and RSC-Energia. In 1998, he established the Draper graduate student fellow program at Rice University and has graduated 16 M.Sc. Fellows. He is the recipient of the 2008 NASA Exceptional Public Service Medal for expanding ISS flight control system capabilities. He has led technology innovation in computational control design

for flexible spacecraft, real- and nonreal-time trajectory design, CMG steering laws and singularity analysis, network centric computing, rapid modeling, and simulation development. He received a B.S.M.E. from the University of Florida and SM. and Ph.D. degrees from Massachusetts Institute of Technology, in mechanical engineering. He can be contacted at Manned Space Systems, The Charles Stark Draper Laboratory, 17629 El Camino Real, Suite 470, Houston, TX 77058 USA.

Sagar Bhatt is a member of the technical staff at the Charles Stark Draper Laboratory in Houston, Texas. For ISS, his responsibilities include zero-propellant maneuver design, certification, and implementation in the ISS Timeliner procedure scripting user interface language. As part of the Shuttle flight readiness certification team, he performs thruster control systems verification and provides mission support. He received a B.S. in mathematics from Texas A&M University in 2004 and an M.A. in computational and applied mathematics from Rice University in 2007 while a Draper graduate fellow.

Wei Kang received the Ph.D. in mathematics from the University of California at Davis in 1991. From 1991 to 1994, he was a visiting assistant professor of systems science and mathematics at Washington University in St. Louis. In 1994, he joined the faculty of applied mathematics at the Naval Postgraduate School, where he is currently a professor of applied mathematics. He is also a director of the American Institute of Mathematics. His research interests include computational mathematics in control design, bifurcations and normal forms, H-infinity control, manufacturing and process control, autonomous vehicles, and space systems. He was a plenary speaker at two international conferences organized by SIAM and IFAC. He is an IEEE Fellow and a member of SIAM.

I. Michael Ross is a professor and program director of control and optimization at the Naval Postgraduate School. He is the principal investigator on pseudospectral feedback control experiments onboard various satellites sponsored by AFOSR, AFRL, AFTENCAP, DARPA, and SPAWAR. He received the Ph.D. in aerospace engineering from the Pennsylvania State University. As a visiting professor at the Charles Stark Draper Laboratory from 1999 to 2001, he introduced pseudospectral methods for nonlinear control problems in the areas of launch and entry guidance, attitude control, and inertial navigation. He is the author of DIDO, a software package for solving optimal control problems. An associate fellow of the AIAA and the founding book review editor for the *Journal of Guidance, Control and Dynamics*, his research interests are in real-time computation of optimal control, low-thrust orbital maneuvers, aero-braking, spacecraft singularity-free control, and missile guidance.

REFERENCES

[1] N. Bedrossian, S. Bhatt, M. Lammers, L. Nguyen, and Y. Zhang, "First ever flight demonstration of Zero Propellant Maneuver attitude control concept," in *Proc. 2007 AIAA GN&C Conf.,* Hilton Head, SC, Aug. 20–23, 2007, AIAA 2007-6734, pp. 1–12.

[2] S. Bhatt and N. Bedrossian (2007, Nov. 19). First-ever space station Zero-Prop Maneuver (ZPM). [Online]. Available: http://www.youtube.com/watch?v=MIp27Ea9_2

[3] N. Bedrossian, S. Bhatt, M. Lammers, and L. Nguyen, "Zero Propellant Maneuver flight results for 180° ISS rotation," in *Proc. 2007 Int. Symp. Space Flight Dynamics,* Annapolis, MD, Sept. 24–28, 2007, NASA/CP-2007-214158, pp. 1–10.

[4] S. Bhatt and N. Bedrossian (2007, Nov. 19). 180 deg space station Zero-Prop Maneuver (ZPM). [Online]. Available: http://www.youtube.com/watch?v=kyPNzVZy36M

[5] N. Bedrossian, S. Bhatt, A. Alaniz, E. McCants, L. Nguyen, and G. Chamitoff, "ISS contingency attitude control recovery method for loss of automatic thruster control," in *Proc. 31st AAS Guidance and Control Conf.,* Breckenridge, CO, Feb. 1–6, 2008, AAS 08-001, pp. 3–16.

[6] J. Pietz. (2003, Apr.). Pseudospectral collocation methods for the direct transcription of optimal control problems. Master's thesis., Dept. Comput. Appl. Math., Rice Univ., Houston, TX [Online]. Available: http://www.caam.rice.edu/tech_reports/2003/TR03-10.pdf

[7] P. C. Hughes, *Spacecraft Attitude Dynamics.* New York: Wiley, 1986.

[8] J. R. Wertz, Ed., *Spacecraft Attitude Determination and Control.* Boston: Dordrecht, 1978.

[9] W. B. Chubb and S. M. Seltzer, "Skylab attitude and pointing control system," NASA TN D-6068, Feb. 1971.

[10] T. R. Coon and J. E. Irby, "Skylab attitude control system," *IBM J. Res. Develop.,* vol. 20, no. 1, pp. 58–66, 1976.

[11] B. K. Powell, "Gravity gradient desaturation of a momentum exchange attitude control system," in *Proc. AIAA Guidance, Control and Flight Mechanics Conf.,* Hempstead, NY, Aug. 16–18, 1971, AIAA 71-940.

[12] D. Tong, "Spacecraft momentum dumping using gravity gradient," *J. Spacecraft Rockets,* vol. 35, no. 5, pp. 714–717, Sept./Oct. 1998.

[13] C. D. Johnson and R. E. Skelton, "Optimal desaturation of momentum exchange control systems," *AIAA J.,* vol. 9, no. 1, pp. 12–22, Jan. 1971.

[14] G. Chamitoff, A. Dershowitz, and A. Bryson, "Command level maneuver optimization for the International Space Station," in *Proc. AAS Guidance and Control Conf.,* Breckenridge, CO, Feb. 2–6, 2000, AAS 00-027, pp. 311–326.

[15] B. R. Hoelscher and S. R. Vadali, "Optimal open-loop and feedback control using single gimbal control moment gyroscopes," *J. Astronaut. Sci.,* vol. 42, no. 2, pp. 189–206, Apr./June 1994.

[16] B. Wie, *Space Vehicle Dynamics and Control.* Reston, VA: AIAA, 2008.

[17] N. Bedrossian and E. McCants, "Space station attitude control during payload operations," in *Proc. AAS/AIAA Astrodynamics Conf.,* Girdwood, AK, Aug. 16–19, 1999, pp. 1083–1094.

[18] Elissar, Monterey, CA.. DIDO [Online]. Available: http://www.elissar.biz/

[19] I. M. Ross and Q. Gong, "Guess-free trajectory optimization," in *Proc. AIAA Guidance, Navigation and Control Conf.,* Honolulu, HI, Aug. 18–21, 2008, AIAA Paper 2008-6273, pp. 1–15.

[20] N. Bedrossian and S. Bhatt, "Space station zero-propellant maneuver guidance trajectories compared to eigenaxis," in *Proc. 2008 American Control Conf.,* Seattle, WA, June 11–13, 2008, pp. 4833–4838.

[21] N. Bedrossian, "Better—50× faster—$12M cheaper: An example from ISS GN&C systems Flight Readiness Certification," in *Proc. 2004 AIAA Modeling and Simulation Technologies Conf.,* Providence, RI, Aug. 16–19, 2004, AIAA 2004-5271, pp. 1–10.

[22] J. Oberg. (2007, Oct.). Space station: Internal NASA reports explain origins of June computer crisis. *IEEE Spectr.,* vol. 44, no. 10. [Online]. Available: http://www.spectrum.ieee.org/oct07/5598.

[23] R. Lee, S. Gomez, and G. W. Vajdos, "Manual GN&C redundancy management techniques during ISS Russian computer failures," in *Proc. 31st AAS Guidance and Control Conf.,* Breckenridge, CO, Feb. 1–6, 2008, AAS 08-074, pp. 617–626.

[24] N. Bedrossian, J.-W. Jang, A. Alaniz, M. Johnson, K. Sebelius, and Y. Mesfin, "International Space Station US GN&C attitude hold controller design for Orbiter Repair Maneuver," in *Proc. AIAA GN&C Conf.,* San Francisco, CA, Aug. 15–18, 2005, AIAA-2005-5853, pp. 1–15.

[25] S. Bhatt. (2007, May). Optimal reorientation of spacecraft using only control moment gyroscopes,. Master's thesis., Dept. Comput. Appl. Math., Rice Univ., Houston, TX. [Online]. Available: http://www.caam.rice.edu/tech_reports/2007/TR07-08.pdf